MSc. Thesis

Wave runup on atoll reefs

Ellen Quataert
January 2015

Deltares Enabling Delta Life

TU Delft Delft University of Technology

USGS science for a changing world

Front cover: Aerial view of the southern tip of the Kwajalein Atoll in the Republic of the Marshall Islands.
Source: www.fayeandsteve.com

Deltares

Wave runup on atoll reefs

Ellen Quataert

1210070-000

Keywords
Runup, atoll reef, XBeach, infragravity wave, wave-induced setup, incident swash, infragravity swash, Kwajalein

Summary
The aim of this research was to take the first step in understanding the wave runup process on an atoll reef using the XBeach model. Field data collected from 3 November 2013 to 13 April 2014 at Kwajalein Atoll in the Republic of the Marshall Islands was used. The dataset included data on bathymetry, waves, water levels and wave-induced runup. The data was analysed and subsequently used to model the hydrodynamics across the reef and the wave runup. The hydrostatic and non-hydrostatic XBeach models were used to capture both components of runup, infragravity and incident swash. Finally, a conceptual model was created to investigate the effect of variations in the atoll reef parameter space on the wave runup.

References
1210070-000

Version	Date	Author	Initials	Review	Initials	Approval	Initials
	Jan. 2015	E. Quataert		A.R. van Dongeren		F. Hoozemans	
				A.A. van Rooijen			

State
final

Deltares

Wave runup on atoll reefs

by Ellen Quataert

in partial fulfilment of the requirements for the degree of

Master of Science
in Civil Engineering

Delft University of Technology
January 2015

In collaboration with:

Graduation committee:

Prof. dr. ir. M.J.F. Stive	Delft University of Technology
ir. A.A. van Rooijen	Deltares / Delft University of Technology
dr. C.D. Storlazzi	USGS-Pacific Coastal and Marine Science Center
dr. ir. A.R. van Dongeren	Deltares
dr. ir. M. Zijlema	Delft University of Technology

Abstract

Coral reefs are capable of protecting mainland and island coasts from the impacts of severe storm waves and storm surges, the impact of tsunamis, and help limit coastal erosion. Despite the protective capabilities of coral reefs, coastlines fronted by coral reefs are still threatened by the ocean. For example, a series of inundation events on islands across the western Pacific (e.g. Wake Atoll, Guam and Kwajalein Atoll) in December 2008 resulted in severe damage on the islands. Many of these islands are low-lying atolls and have maximum elevations of 3 to 5 m above mean sea level. An atoll is a circular reef that, partially, encloses a lagoon which can contain a freshwater lens. Wave-induced overwash and inundation threatens infrastructure and freshwater resources, which has consequences on the suitability of the islands for agriculture and habitation. The inundation events resulted in the need for a better understanding of the processes causing these inundation events on atoll islands. An investigation on this matter is carried out by the joint U.S. Geological Survey (USGS), National Oceanographic and Atmospheric Administration (NOAA) and University of Hawaii. The primary goal of the investigation is to determine the influence of sea-level rise on wave driven inundation and the resulting impacts to infrastructure and freshwater resources on atoll islets in the Pacific and Indian Oceans.

Coasts fronted by (coral) reefs have some important physical differences with sandy coasts. The steep fore reef, the relatively long and shallow reef flat and the higher bottom roughness enforces specific hydrodynamic processes. The resulting water level variations, wave propagation and forcing across the reef and the wave-induced runup are the main processes driving inundation events. The majority of the studies that have been conducted have focused on the hydrodynamics across reefs. Little is known about the wave-induced runup in the presence of a reef. Therefore, the aim of this thesis was to take the first step in understanding the wave runup process on an atoll reef using the XBeach model.

In this study, field data collected from 3 November 2013 to 13 April 2014 at Kwajalein Atoll in the Republic of the Marshall Islands was used. The dataset included measurements on bathymetry, waves, water levels and wave-induced runup. The data was analysed and subsequently used to model the hydrodynamics across the reef and the wave runup. The hydrostatic and non-hydrostatic XBeach models were used to capture both components of runup, infragravity and incident swash. Finally, a conceptual model was generated to investigate the effect of variations in the atoll reef parameter space on the wave runup.

The data was analysed to derive the wave heights, wave-induced setup and wave runup along the cross-shore reef profile. The wave height evolution over the reef towards the shore showed a general trend of increasing low frequency (infragravity and very low frequency) waves and decreasing high frequency (short) waves. Especially during the energetic wave events, the IG and VLF wave heights increase substantially and became dominant near the shoreline. Furthermore, it was found that on the reef flat the wave heights, wave-induced setup and wave runup are all strongly affected by the offshore tidal variations. Runup observations were collected for the period between 3 November 2013 and 17 December 2013 and included one extreme runup event on 17 November at 16:17.

The extreme wave runup event on the Kwajalein Atoll is significantly underestimated by the hydrostatic XBeach model. The non-hydrostatic model includes the incident swash in the simulations and showed an improved wave runup prediction, despite the underestimated

wave-induced setup. However, still a clear underestimation of the wave runup was found, which was explained by an instantaneous increase in surface elevation in the raw burst of data at the inner reef flat pressure sensor. For the measured extreme wave runup event at Kwajalein Atoll, it is therefore not sufficient to schematize the hydraulic conditions into hourly burst-averaged characteristics for this specific event.

The XBeach hydrostatic model showed good results for the hydrodynamics across the reef, but the non-hydrostatic model performed better on the wave runup. Extrapolating these results to storm conditions, it is expected the contribution of the incident swash to the total wave runup increases significantly, as the water depth on the reef flat increases. This effect was substantiated by the conceptual model simulations. Furthermore, the impact of incident swash is expected to become stronger considering the effects of rising sea levels. However, further investigation is needed on the underestimation of the wave-induced setup on the reef flat by the non-hydrostatic model. If this issue can be solved, the non-hydrostatic model is capable to model the wave runup (and subsequently inundation events) more accurately.

Acknowledgements

With this thesis the Master of Science programme at Delft University of Technology is completed. The research was carried out at Deltares in Delft and USGS-Pacific Coastal and Marine Science Center in Santa Cruz, California.

I would like to greatly thank my graduation committee for their support and enthusiasm throughout my thesis. My daily supervisors at Deltares, Ap van Dongeren and Arnold van Rooijen, for their inspiring and skilled supervision and the time they invested in me. Thanks to Marcel Stive and Marcel Zijlema for their enthusiasm and guidance during the meetings we had. Special thanks to Curt Storlazzi for the guidance during my stay in Santa Cruz. Your enthusiasm for this research was very encouraging. I have learned a lot about coral reef hydrodynamics and modelling for which I thank you all.

I had the opportunity to spend three months within this research at the U.S. Geological Survey in Santa Cruz, California. Many thanks to the USGS and Deltares for giving me this opportunity, it has been a unforgettable and valuable experience. Many thanks to everyone at the USGS in Santa Cruz for making me feel at home in Santa Cruz. Special thanks to Olivia Cheriton for the help and the interesting conversations we had on data analysis.

Finally, and most importantly, I would like to thank my parents and sisters for the continuous support, encouragements and patience throughout my study.

Ellen Quataert
Delft, January 2015

Contents

1 Introduction

1.1 Background

Coral reefs are capable of protecting mainland and island coasts from the impacts of severe storm waves and storm surges, the impact of tsunamis, and help limit coastal erosion (e.g. Ferrario et al., 2014). Coral reefs can be found in the open ocean and along coasts in tropical and subtropical waters. Based on topography three types of coral reefs can be distinguished; barrier, fringing and atoll reefs (Darwin, 1842). A barrier reef is characterized by a deep lagoon in the lee side of the reef. Consequently the reef is detached from the land. A fringing reef is connected to the shoreline and can have a shallow lagoon at the lee side of the reef. An atoll island is a circular reef that, partially, encloses a lagoon which can contain a freshwater lens.

Despite the protective capabilities of coral reefs, coastlines fronted by coral reefs are still threatened by the ocean. A series of inundation events on islands across the western Pacific during December 2008 resulted in severe damage on the islands. Many of these Pacific islands are low-lying atolls fronted by coral reefs and have maximum elevations of 3 to 5 m above mean sea level. Wave-induced overwash and inundation threatens infrastructure and freshwater resources, which has consequences on the suitability of the islands for agriculture and habitation. The inundation events of December 2008 have been investigated by Hoeke et al. (2013). It was proven that the main cause of the inundation events was a large swell generated in the northern Pacific Ocean. Additionally, the sea level elevation due to climate change related sea level rise and La Nina conditions also played an important role in the inundation events. These events resulted in the need for a better understanding of the processes causing these inundation events on atoll islands.

An investigation on this matter is carried out by the joint U.S. Geological Survey (USGS), National Oceanographic and Atmospheric Administration (NOAA) and University of Hawaii. The primary goal of the investigation is to determine the influence of sea-level rise on wave driven inundation and the resulting impacts to infrastructure and freshwater resources on atoll islets in the Pacific and Indian Oceans. One direct application is to provide understanding and information on the inundation of atoll islands with US Department of Defence (DOD) installations. Kwajalein Atoll in the Republic of the Marshall Islands is such an atoll and is used as a test case in the investigation. On the Kwajalein atoll instruments were deployed to collect field data for validating and calibrating the physics-based, numerical wave and water-level models. Once the present conditions at Kwajalein Atoll are accurately reproduced by the models, predictive modelling will be conducted of sea level rise impact on infrastructure and freshwater resources. Additionally, the knowledge gathered on the Kwajalein Atoll will provide insight into the impact of climate change on atoll systems throughout the Pacific and Indian Oceans.

Coasts fronted by coral reefs have some important physical differences with sandy coasts which enforces specific hydrodynamic processes. Water level variations, wave propagation and forcing across the reef and runup are the main processes driving inundation events. The majority of the studies that have been conducted have focused on the wave-induced hydrodynamics across (coral) reefs. Little is known about the wave-induced runup in the presence of a (coral) reef.

1.1.1 Hydrodynamics on reefs

The ocean side of a typical atoll reef is generally characterized by a steep fore reef slope, a relatively long reef flat with respect to the water depth and rough bottom topography. In comparison to a sandy coast, with a mild slope and smooth bed profile, reefs will force different hydrodynamics associated with waves.

Short wave dynamics on reefs have been studied extensively. The steep slope of the fore reef and the long reef flat induces wave breaking at a relatively large distance from the shoreline. During a field and desktop study at Bikini Atoll Munk and Sargent (1948) showed this resulted in a mean wave setup of several decimetres. This setup can be explained by the spatial gradients in radiation stress due to wave breaking which is balanced by a gradient in the water level over the reef flat (Longuet-Higgins & Stewart, 1962).

Lee and Black (1978) and Young (1989) studied the transformation of incident short waves across coral reefs and found the significant wave height depends on the water depth on the reef and the offshore wave conditions. Additionally, they found a significant broadening of the spectrum during propagation across a reef. It was speculated the presence of surf beats caused a spectral redistribution from higher to lower frequencies.

Many laboratory (e.g. Gerritsen, 1980; Gourlay, 1996; Seelig, 1983) and field studies (e.g. Becker, Merrifield, & Ford, 2014; Vetter, Becker, & Merrifield, 2010) have been conducted on the water level setup on reef flats. Gerritsen (1980) and Gourlay (1996) conducted laboratory experiments to measure wave induced setup on a fringing reef. They both generated a dimensionless representation of the wave setup. Seelig (1983) conducted laboratory experiments on a idealized reef-lagoon system. He found among others as the water level on the reef flat decreases, the setup increases with a wave energy flux parameter. He also found the lagoon width did not influence the setup. Vetter et al. (2010) used the observed setup on a fringing reef at Ipan, Guam and showed that predictions based on the traditional setup theory (Longuet-Higgins & Stewart, 1962) and an idealized point break model of wave transformation are in agreement with observations. Becker et al. (2014) considered the impact of tidal variations on wave setup over fringing reefs, using field measurements obtained at three sites at Majuro Atoll, Kwajalein Atoll and Guam in the western tropical Pacific Ocean. They found a tidal dependence of the wave-induced setup due to tidally dependent wave breaking on the fore reef.

Lowe (2005) conducted a field experiment to measure wave dissipation on a barrier reef at Kaneohe Bay, Hawaii. He found the majority of the wave energy dissipation was caused by bottom friction instead of wave breaking. This is in contrast to the previous assumptions of dissipation on coral reefs, where wave breaking was more dominant (e.g. Lee & Black, 1978; Young, 1989). Additionally, it was found the variation of the dissipation by bottom friction could be described by a hydraulic roughness length scale.

The observed shift in energy towards lower frequencies by (Young, 1989) and (Lee & Black, 1978) indicated the importance of low frequency waves on a coral reef. The low frequency wave motions, or infragravity waves, are driven by the temporal variation of wave height on the wave-group scale. The generation of these long waves can be explained by the bound long wave concept (Longuet-Higgins & Stewart, 1962) and the breakpoint generation mechanism (Symonds, Huntley, & Bowen, 1982). Longuet-Higgins and Stewart (1962) combined the low frequency wave with the short wave radiation stress and mass flux and concluded the low frequency wave travels with the short wave group velocity, creating the bound long wave. Symonds et al. (1982) proposed the point of breaking varies spatially due

to a varying wave height in time. This moving breakpoint generates waves at the group period, hence creating infragravity waves in the surfzone. This breakpoint forcing mechanism is thought to become more important as the relative slope at the breakpoint is large.

Most recent field studies have shown that the contribution of short waves to the surface elevation on a reef flat is significantly small compared to the contribution of the infragravity waves (Péquignet, Becker, Merrifield, & Aucan, 2009) and (Pomeroy, Lowe, Symonds, van Dongeren, & Moore, 2012). Péquignet et al. (2009) observed low frequency near resonant oscillations dominated the surface elevation during tropical storm Man-Yi on the Ipan reef in Guam. Pomeroy et al. (2012) found for a fringing reef at Ningaloo Reef in Western Australia that the steep fore reef generates free infragravity waves by breakpoint forcing. Additionally due to the strong dissipation of infragravity waves, the at the shoreline reflected seaward propagating infragravity waves were small. Hence, progressive shoreward propagating infragravity waves dominate on the reef flat.

1.1.2 Runup

Runup is defined as the vertical excursion of the water level at the shoreline relative to the still-water level (SWL) and is commonly represented by the runup value that is exceeded 2% of the time, $R_{2\%}$ (Holman, 1986). This statistic is often used as the extreme values are of interest in engineering applications. Hunt (1959) suggested the relative runup level, $R_{2\%}/H_{m0}$, is linearly dependent of the surf similarity parameter ξ:

$$\frac{R_{2\%}}{H_{m0}} = \xi \qquad [1.1]$$

where H_{m0} is the significant wave height at the toe of a structure. The surf similarity parameter, or Iribarren number (Battjes, 1974), describes the relative steepness of the beach slope with respect to the incoming wave:

$$\xi = \frac{\beta}{\sqrt{H_{m0} / L_0}} \qquad [1.2]$$

where β is the beach slope and L_0 is the deep water wave length. A high Iribarren number (>5) represents a reflective beach and a low Iribarren number (< 0.5) represents a dissipative beach.

Runup can be separated into two components; wave setup and an oscillatory component, swash (Holman, 1986). The wave induced setup (section 1.1.1) component in runup is the time-averaged water level elevation at the shoreline. Swash is defined as the time-varying vertical fluctuations about the setup and has two types of motions. The first is high frequency swash (incident-band swash), generated by dissipating waves. The second is low frequency swash (infragravity swash), generated by non-breaking infragravity waves that reflect at the beach and act as standing waves.

There are many empirically derived formulations for determining the magnitude of runup on sandy coasts and structures such as breakwater, revetments and dikes. These formulations are mostly a function of the Iribarren number, as in equation [1.1], including multiple dimensionless factors based on the analysis of observations of offshore wave conditions and runup measurements (e.g. Holman, 1986; TAW, 2002).

One of the most used empirical formulations for runup on sandy beaches is derived by (Stockdon, Holman, Howd, & Sallenger, 2006) and include a formulation for each component of runup. These empirical formulations were defined using statistics from 10 field experiments on sandy beaches under different environmental conditions. This resulted in the following empirical relations;

$$
\begin{aligned}
R_{2\%} &= 1.1 \cdot \left[\bar{\eta} + \frac{S}{2} \right] \\
\bar{\eta} &= 0.35 \beta \sqrt{H_0 L_0} \\
S &= \sqrt{\left(S_{inc}\right)^2 + \left(S_{IG}\right)^2} \\
S_{inc} &= 0.75 \beta \sqrt{H_0 L_0} \\
S_{IG} &= 0.06 \sqrt{H_0 L_0}
\end{aligned}
\qquad [1.3]
$$

where $\bar{\eta}$ is the time-averaged water level elevations at the shoreline (i.e. setup), H_0 the deep water wave height, S is the total swash, S_{IG} is the infragravity swash and S_{inc} the incident swash. The setup at the shoreline and the incident swash are best parameterized using a dimensional form of the Iribarren parameter according to equation [1.3]. The infragravity swash is only influenced by the offshore wave height and wave length.

Currently, there is no empirical formula for runup in a reef environment. Seelig (1983) conducted a laboratory study and presented results of wave runup height. He noted low-frequency oscillations were dominant in the maximum runup values. Nwogu and Demirbilek (2010) modelled the runup and infragravity wave motions over a fringing reef using a Boussinesq model and laboratory experiments. They found that although the wave induced set-up decreased, the wave runup increased with increasing water level. This was caused by the dominance of the infragravity oscillations. A quadratic dependence of maximum runup height with the surf similarity parameter was suggested. However, the laboratory flume experiments were conducted with smooth bottom beds resulting in a minimal bottom friction in the model. Therefore, the effect of bottom friction on the waves is not taken into account but can have a significant effect on reef hydrodynamics as was proven by Lowe et al. (2005).

1.1.3 Terminology

In this section the terminology used throughout this thesis is defined. The focus of this study is on the hydrodynamics along a one-dimensional atoll reef profile. An idealized one-dimensional cross-shore profile of an atoll reef is shown in Figure 1.1, where the key features of atoll reefs are defined (i.e. fore reef, reef flat and beach).

In addition, in Figure 1.1 the definition of wave runup and its components are presented. The offshore tidal elevation can be below the reef flat level, which has a significant effect on the terminology regarding atoll reefs. Figure 1.1 shows the definition of wave-induced setup (η_{setup}) and wave runup ($R_{2\%}$) for both an offshore water level above and below the reef flat level. The runup value during the lower offshore water level is significantly higher, although the vertical water level excursion on the beach is exactly the same. Therefore, in this study a reference level is set at the reef flat level, in order to consistently compare the hydrodynamics parameters. Every hydrodynamic parameter (e.g. mean offshore water level ($\overline{\eta}_{offshore}$), mean water level ($\overline{\eta}$) and 2% exceedence level of wave runup ($z_{2\%}$)) is defined with respect to this reference level.

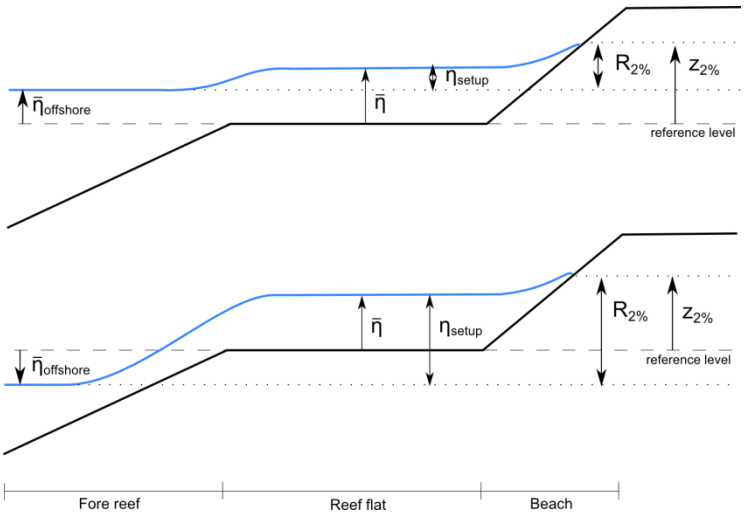

Figure 1.1 Idealized 1D cross-shore profile of an atoll reef including key features and the definition of wave runup and its components: mean offshore water level ($\overline{\eta}_{offshore}$), mean water level ($\overline{\eta}$),wave-induced setup ($\eta_{setup}$), wave runup ($R_{2\%}$) and 2% exceedence level of wave runup ($z_{2\%}$).

1.2 Scope and objectives of this study

As elaborated previously, numerous studies have been conducted on the high and low frequency wave motions on a reef. Also various studies have been carried out on runup processes on sandy beaches and coastal structures. However, the knowledge of wave runup on coastlines fronted by (coral) reefs is limited.

This thesis will focus on atoll type reef structures and will take the first step in understanding the wave runup process on an atoll reef using the XBeach model (Roelvink et al., 2009). The scope of the present study is on the hydrodynamic processes along a one-dimensional atoll reef profile. To obtain reliable results from the XBeach simulations, the hydrodynamic and runup field data of the Kwajalein Atoll is used to calibrate and validate the model. The primary objective of the present study is therefore;

Understanding wave runup processes on atoll reefs using the XBeach model

In order to accomplish the main objective the following secondary objectives are formulated:

- Analysis of the Kwajalein Atoll field data for the hydrodynamics across the reef and wave runup;
- calibrating and validating the XBeach model for the hydrodynamics across the reef with the Kwajalein Atoll field data;
- using the calibrated and validated XBeach model to reproduce the wave runup and validate with the wave runup Kwajalein data;
- generate an idealized cross-shore atoll reef profile and test the sensitivity of the wave runup to variations in the parameter space.

1.3 Thesis outline

This study comprises roughly three parts: Kwajalein Atoll data analysis (chapter 2), numerical modelling of the wave runup on Kwajalein Atoll (chapter 3 and 4) and conceptual modelling of wave runup on atoll reefs (chapter 5).

In chapter 2, the obtained data at Kwajalein Atoll is presented and analysed to capture the hydrodynamic processes which are relevant in reef environments. Chapter 3 provides a description of the XBeach model and its applicability for the particular case of a reef environment. In chapter 4 the capability of the XBeach model to simulate the hydrodynamics across the reef and wave runup at the Kwajalein atoll reef is tested. Chapter 5 the sensitivity of wave runup to variations in the atoll reef parameter space is tested by creating an idealized one-dimensional cross-shore profile of an atoll reef. Finally, the conclusions and recommendations of this study are presented in chapter 6.

2 Kwajalein Atoll data analysis

2.1 Introduction

The Kwajalein Atoll is part of the Republic of the Marshall Islands in the Pacific Ocean (Figure 2.1), and is an atoll system with islands that surrounds a large lagoon which includes a freshwater lens. The Roi-Namur Island is located at the northern tip of Kwajalein Atoll and is selected as study site to investigate the influence of sea level rise on wave driven inundation on atoll islets in the Pacific and Indian Oceans. On the Roi-Namur Island instruments were deployed from 3 November 2013 to 17 December 2013 to collect field data on bathymetry, waves, water levels and wave runup.

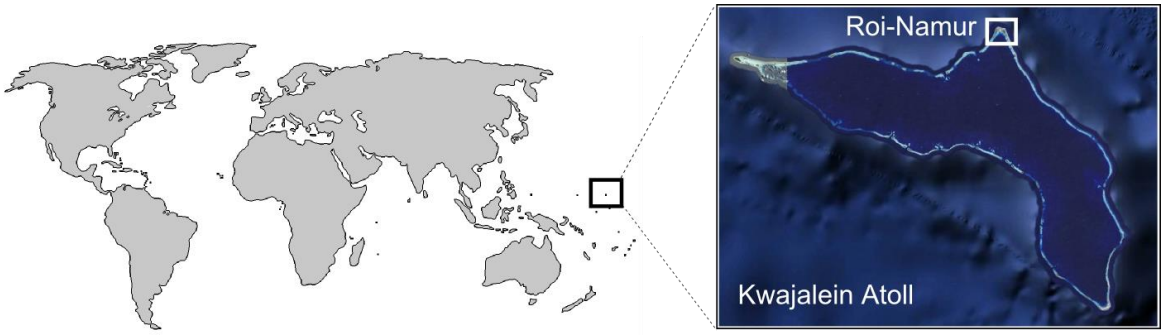

Figure 2.1 Location of the Kwajalein Atoll (RMI) in the Pacific Ocean and the Roi-Namur island at Kwajalein Atoll.

In this chapter the data obtained during the field experiment is presented and analysed to capture the hydrodynamic processes which are relevant in reef environments. First a description of the study site and an overview of the instrument deployment are presented in section 2.2. In section 2.3 the hydrodynamic data across the reef is presented and analysed. Next, the wave runup data is presented and analysed in section 2.4. In section 2.5 a discussion regarding the results is given and finally the main conclusions from this chapter are presented in section 2.6.

2.2 Study site and instrument deployment

During the field experiment from 3 November 2013 to 13 April 2013 on the Roi-Namur island an array of four pressure sensors were deployed along two cross-shore transects, in North-East (NE) and North-West (NW) direction. On each transect three pressure sensors were deployed on the reef flat and one on the fore reef. A Nortek Acoustic Wave and Current profiler (AWAC) located offshore provided deep water wave conditions for both transects. Additionally, a digital time-lapse camera was installed along the coastline to collect runup data. The bathymetry was measured prior to the hydrodynamic measurements. Because data was lost of the fore reef pressure sensor at the NE transect the present study will focus on the data obtained at the NW transect. In Figure 2.2 an overview of the instrument locations and bathymetry profile is given and in Table 2.1 the instrument and measurement details are summarized.

The offshore AWAC was located at 20 m below the mid reef crest level. On the fore reef a pressure sensor was located at a depth of 7 m. From this point the fore reef consists of a slope of approximately 1:20 and has an irregular and rough topography as it is covered by corals. From the most offshore located measurement location up to the outer reef flat pressure sensor the high energy wave conditions prevented direct depth measurements. For these sections of the bathymetry a linear interpolation between the known points was made. The reef crest is connected to the coastline of the islet by a reef flat under a very gentle slope (1:110 slope). The 250 meter long reef flat has a relatively smooth surface and is covered by a relatively small amount of coral rubble. As the shallow reef flat is exposed during low tide, it is impossible for corals to grow on the reef flat. At the coastline a relatively steep sandy beach (1:6 slope) connects the reef flat to the low-lying atoll islet.

The AWAC and pressure sensors were deployed between 3 November 2013 and 13 April 2014. All hydrodynamic data were collected at a burst interval of one hour with a burst duration of 2048 s. The sample frequency was set at 1 Hz for the AWAC and at 2 Hz for the pressure sensors.

Wave runup data was collected with a digital time-lapse camera located on the beach, indicated in Figure 2.2 with the ‘x’. Photos were taken every 30 minutes of the beach in seaward direction. Wave runup data is collected for the period between 3 November 2013 and 17 December 2013 only.

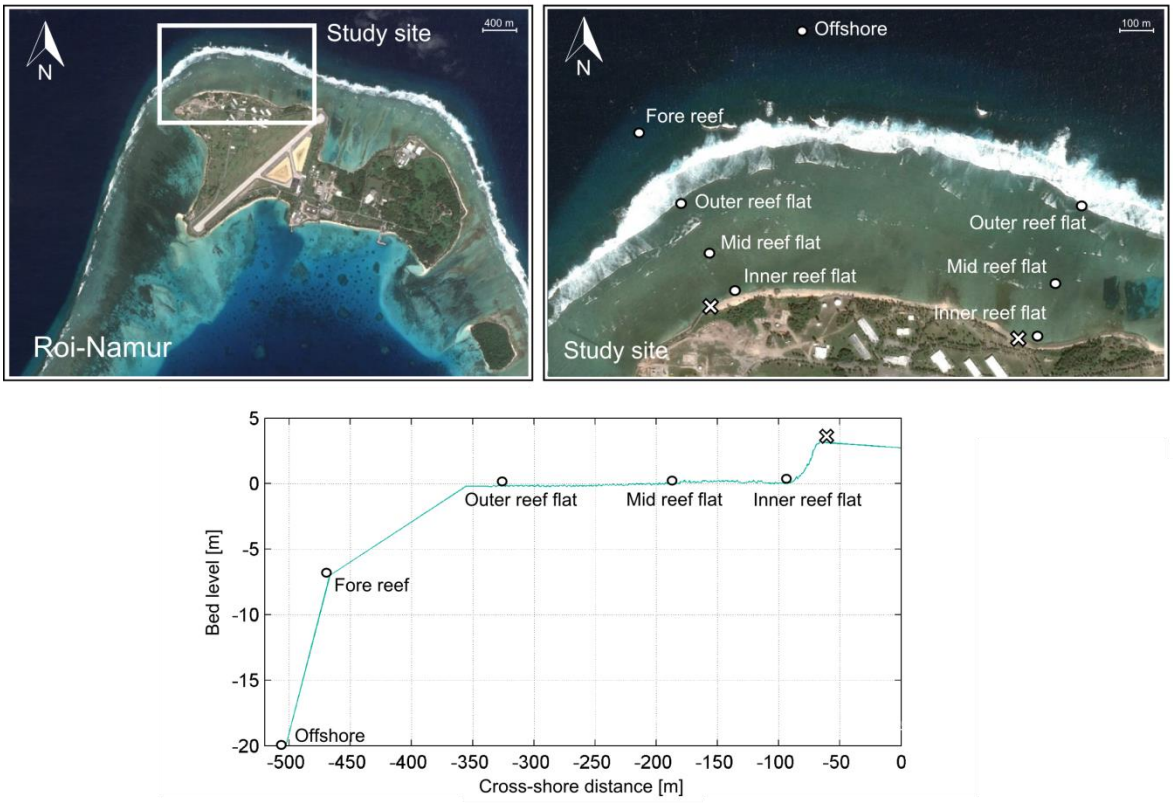

Figure 2.2 Top view of Roi-Namur (top left). Study site (top right) and bathymetry profile along the cross-shore instrument transect (bottom), both with instrument locations shown. The 'x' indicates the location of the digital time-lapse camera for the runup observations.

Table 2.1 Instrument configuration used for data collection

Location	*Instrument*	*Measurement rate*	*Type of data*
Offshore	Nortek AWAC	Hourly 2048s bursts at 1 Hz	Pressure and velocity
Fore reef	RBR virtuoso	Hourly 2048s bursts at 2 Hz	Pressure
Outer reef flat	RBR virtuoso	Hourly 2048s bursts at 2 Hz	Pressure
Mid reef flat	RBR virtuoso	Hourly 2048s bursts at 2 Hz	Pressure
Inner reef flat	RBR virtuoso	Hourly 2048s bursts at 2 Hz	Pressure
Beach	Digital time-lapse camera	One photo every 30 min	Maximum runup height

2.3 Hydrodynamics across the reef

The typical features of coasts fronted by reefs, such as shallow reef flat and high bottom roughness, results in specific hydrodynamic processes across the reef. As discussed in section 1.1.1, many studies have investigated the relevant hydrodynamic processes in reef environments. To obtain insight into the relevant hydrodynamic processes at Kwajalein Atoll, the obtained data from the field experiment presented in section 2.2 is analysed in this section. First, the methodology for data processing will be described. Subsequently the offshore wave conditions, water level variations across the reef, split frequency and the spectral evolution across the reef are identified, analysed and compared with results from previous studies.

2.3.1 Methodology

To analyse the hydrodynamic processes across the reef the obtained field data is aggregated into parameters such as water levels, wave heights and wave periods.

First, the pressure time series measured at each location is converted to sea-surface elevation time series, assuming each hourly burst is a stationary signal. For each hourly burst of data a variance density spectrum is generated by applying a Fast Fourier Transform (FFT). The variance density spectrum shows the distribution of the wave energy over different frequencies and is defined as:

$$E(f) = \lim_{\Delta f \to 0} \frac{1}{\Delta f} E\left(\frac{1}{2} \underline{a}^2 \right) \quad [2.1]$$

where Δf is determined by the duration of the burst ($\Delta f = 1/T$) and $\frac{1}{2} \underline{a}^2$ is the variance of the amplitude. However, given the finite duration of each burst of data it is not possible to take the limit $\Delta f \rightarrow 0$. Therefore the spectrum is estimated by band averaging and applying a Hanning window with a 50% overlap to create a smoothed form of the spectrum. To take into account the effects by gradients in the (wave-induced) pressure in the water, a pressure correction factor (K_p) is applied to the spectrum. The linear dispersion relation (equation [2.2]) is used to calculate this pressure correction factor (equation [2.3]).

$$\omega^2 = gk \tanh(kd) \quad [2.2]$$

$$K_p = \frac{\cosh(kz)}{\cosh(kd)} \quad [2.3]$$

where ω is the angular frequency, k the wave number, z the elevation of the measurement instrument above the bed and d the water depth.

The surface elevation time series are treated as a stationary Gaussian process, meaning all its statistical characteristics can be expressed in terms of the moments of the variance density spectrum (Holthuijsen, 2007). The n^{th}-order moment is defined as:

$$m_n = \int_0^\infty f^n E(f) df \quad [2.4]$$

The zero- and first-order moment calculated from equation [2.4] is used to determine the significant wave height (H_{m0}), root-mean-squared wave height (H_{rms}) and mean spectral period (T_{m0}) for each wave burst:

$$H_{m0} = 4\sqrt{m_0}$$
$$H_{rms} = \sqrt{8m_0} \qquad [2.5]$$
$$T_{m0} = \frac{m_0}{m_1}$$

In the generated variance density spectrum both short and long wave energy are present. As discussed in section 1.1.1, in reef environments a spectral evolution over the reef towards the lower frequency has been observed. The separation of the total signal into high and low frequency waves is therefore important in the analysis of the hydrodynamics across the reef.

A distinction between low and high frequency waves can be made using the split frequency (f_{split}). The split frequency should be selected so that leakage of high frequency energy into lower frequency band is avoided. Roelvink and Stive (1989) showed the split frequency can be defined as half of the offshore peak frequency. This means the split frequency changes over time and is affected by the site specific wave climate. In various studies the frequency adopted to split the signal into low and high frequency bands has a value varying from 0.04 Hz to 0.05 Hz. In addition, the low frequency band can be separated into infragravity and very low frequency (VLF) bands. This transition varies with frequencies from 0.004 Hz to 0.005 Hz. Which specific frequency bands are applicable for the Roi-Namur site, is specified in section 2.3.3.

To obtain the short, IG and VLF wave characteristics, the variance density spectrum of each burst is divided into the defined frequency bands as shown in Figure 2.3. Now statistical characteristics of each section of the spectrum, specified by the frequency bands, can be determined. The short, IG and VLF wave heights are obtained by again calculating the zero-order moment of the spectral band, using equations [2.4] and [2.5] with the limits for integration changed for each frequency band.

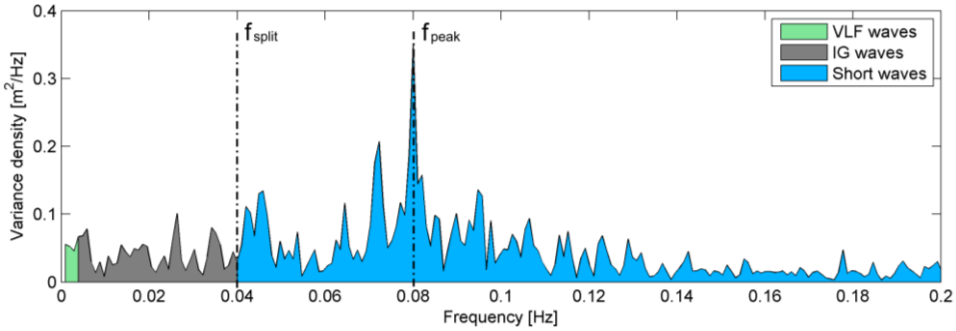

Figure 2.3 Example variance density spectrum including indication of the VLF, IG and short wave frequency bands

2.3.2 Offshore wave conditions

The offshore wave conditions are derived from the pressure and velocity data from the offshore AWAC using the methodology described in the previous section. In Figure 2.4 an overview of the offshore wave conditions of the total deployment period is shown.

The deployment period includes two high energy wave events, on 18 December 2013 and 1 March 2014. The significant wave height during the December event reached 3 m with a peak period of approximately 15 s. The March event resulted in a maximum wave height of even 3.5 m and peak period of 15 s. These events are from here on referred to as the 'December event' and the 'March event'. From local residents it is known that the March event resulted in inundation of the Roi-Namur island. This energetic wave event will therefore be used to analyse the spectral evolution and the water level variations across the reef in the next sections.

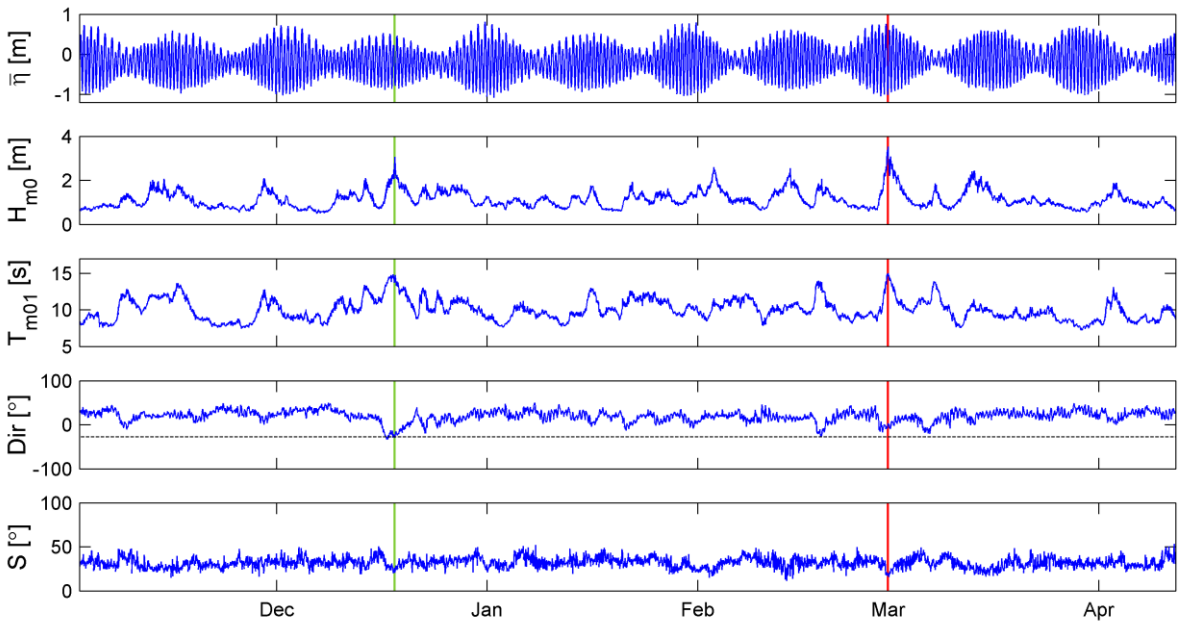

Figure 2.4 Burst-averaged observations of the offshore AWAC. From top to bottom: mean water level (with respect to the mid reef), significant wave height, peak wave period, mean wave direction (from north) and directional spreading. December and March event are indicated by respectively the green and red line.

2.3.3 Split frequency selection

To capture the spectral evolution over the reef, the variance density spectra of each burst of data has to be split into higher and lower frequencies. Using the methodology presented in section 2.3.1, the split frequency (f_{split}) is calculated per burst of data and plotted with the corresponding burst variance density spectrum in the left panels in Figure 2.5. The selected (fixed) split frequency for this specific site is set on 0.04 Hz and is depicted in the right panels in Figure 2.5. This split frequency agrees well with the (strong) transition in variance density magnitude, hence leakage of higher frequency energy to the lower frequencies is avoided. Additionally, in the low frequency band a distinction can be made between an IG and VLF frequency band. The frequency bands adopted in this study are summarized in Table 2.2.

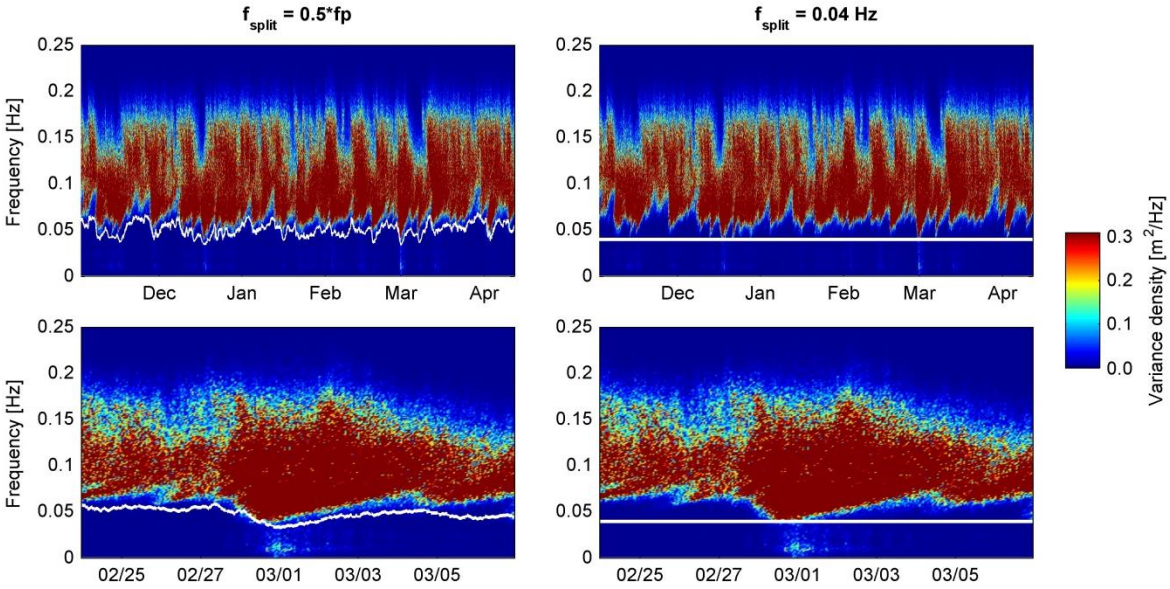

Figure 2.5 Variance density spectra at the offshore instrument for the total deployment period data (top figures) and the March event (bottom figures). The colorbar denotes the variance density in m^2/Hz. The white line represents the split frequency (f_{split}) based on the offshore peak frequency (left panels) and a fixed value of 0.04 Hz (right panels).

Table 2.2 Frequency bands used in this study

High frequency band	0.04 – 0.2 Hz
Infragravity frequency band	0.004 – 0.04 Hz
VLF band	0.001 – 0.004 Hz

2.3.4 Spectral evolution over the reef

With the adopted frequency bands defined in Table 2.2 and using the methodology presented in section 2.3.1 the wave height transformation over the cross-section of the reef is calculated. The results of this separation into short, IG and VLF waves for the March event is shown in Figure 2.6. This section of the data is chosen because it includes an energetic wave event which resulted in overtopping on the Roi-Namur island on 1 March 2014.

Short wave height

Starting at the offshore location the short root-mean-squared wave height increases significantly from 0.5 meter up to 2.7 meter around the 1st of March (the blue line in Figure 2.6). The short wave signals for the offshore and fore reef location have the same shape. The fore reef pressure sensor is located at a depth of 7 meter with respect to the reef flat, so no wave breaking will occur in the area between the offshore AWAC and fore reef pressure sensor for the observed wave heights. However, from the top two plots in Figure 2.6 it can be noticed there is some shoaling of the short waves as the short wave height on the fore reef is slightly higher (approximately 0.20 meter). On the outer reef flat location a rapid reduction in short wave height can be noticed. A significant amount of short wave energy is dissipated primarily through wave breaking along the steep fore reef slope (e.g. Young, 1989). From the outer reef flat to the inner reef flat the short wave height continues to decrease. On the inner reef flat the remaining short wave height is approximately 50% of the short wave height on the outer reef flat. This additional decay of short wave height is largely a result of dissipation by bottom friction (Lowe et al., 2005). Besides, a tidal modulation in the short wave heights is visible, which will be discussed hereafter.

IG wave height

The black line in Figure 2.6 represents the IG root-mean-squared wave height. For the offshore and fore reef locations the IG wave height is very small, with a minor increase during the peak wave event. In contrast with the short waves, the IG wave height increases on the reef flat. On the mid reef flat the IG waves are of the same order of magnitude in height as the short waves. On the inner reef flat the IG waves become even dominant during the peak wave event up to a maximum IG wave height of 0.7 meter. This is in contrast with the results Pomeroy et al. (2012) retrieved at the Ningaloo Reef in Western Australia, where the IG wave height decreased on the reef flat towards the shore due to frictional dissipation. However, the reef flat at the Roi-Namur island is much smoother compared to the Ningaloo reef flat. Frictional dissipation is less important for the IG waves on the Roi-Namur transect, hence the increasing IG wave height towards the beach.

IG energy reaching the beach is either dissipated by breaking and friction or reflected (van Dongeren et al., 2007). As the frictional dissipation of the IG waves is relatively small for the Roi-Namur transect, the remaining IG energy will mainly be reflected at the beach. During the field study at the Kwajalein Atoll no velocities were measured, so no distinction is made between incoming and reflected waves in this study.

VLF wave height

The VLF wave height is shown with the green line in Figure 2.6. The VLF wave height is again very small for the offshore and fore reef locations. On the reef flat the VLF wave heights are small in moderate wave conditions, but increases with the short wave amplitude. During the energetic March event the VLF wave height increases significantly towards the shore and even reaches 0.5 m at the inner reef flat.

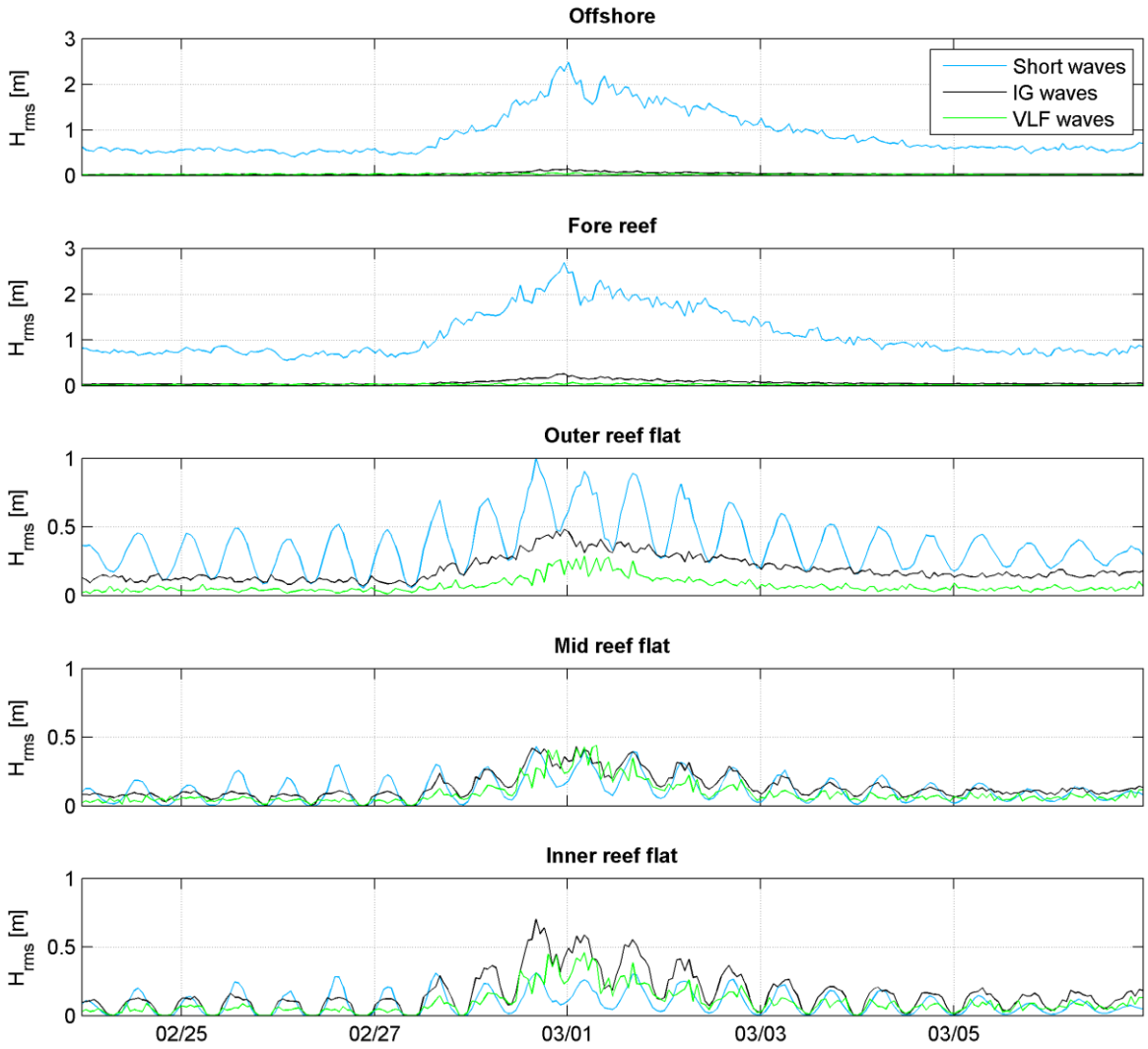

Figure 2.6 The burst-averaged short, infragravity (IG) and Very Low Frequency (VLF) root-mean-squared wave heights for each instrument across the reef.

Tidal modulation

Figure 2.6 shows that the short wave height on the reef flat is strongly controlled by the tidal elevation. In Figure 2.7 the short, IG and VLF wave heights are normalized with the offshore short wave height and plotted as a function of the total water depth on the outer reef flat. The blue dots represent the short wave ratio ($H_{rms}/H_{rms,SW,offshore}$) and indeed responds strongly to the water depth variations. This tidal modulation is because the allowable height of waves increases as the water depth increases on the reef flat. The reef flat falls dry during low tide, so there is no short wave height present on the mid and inner reef flat locations as the water depth approaches zero (Figure 2.7). Similar correlations of the wave height with the tidal elevation have been observed by e.g. Lowe et al. (2005), Péquignet et al. (2011) and Pomeroy et al. (2012).

On the outer reef flat the short wave ratio in Figure 2.7 approaches 1 for higher water depths. These dots represent the normal (moderate wave) conditions (period between 02/25 and 02/27 in Figure 2.6), where the offshore wave height is around 0.5 m. The combination of these relatively small offshore wave heights and high tides leads to the high ratios in Figure 2.7 and means the wave dissipation due to wave breaking on the fore reef is nearly negligible for these conditions.

In Figure 2.7 the IG wave ratio and VLF wave ratio are represented by respectively the black and green dots. Both ratios are roughly constant on the outer reef flat for variations in water depth. On the mid and inner reef flat the ratios for both IG and VLF waves respond strongly to the varying water depth, especially the IG waves on the inner reef flat. The IG and VLF waves are also in phase with the short wave height variations, as can be seen in Figure 2.6. This tidal variability of IG waves is also observed by Pomeroy et al. (2012) at Ningaloo Reef, where a maximum IG wave ratio of only 0.2 was reached. Ningaloo reef is characterized by a much rougher and higher water depths on the reef flat (up to 2.5 m). This suggests that the effect of frictional dissipation on the tidal modulation in IG wave heights is significant on reef flats.

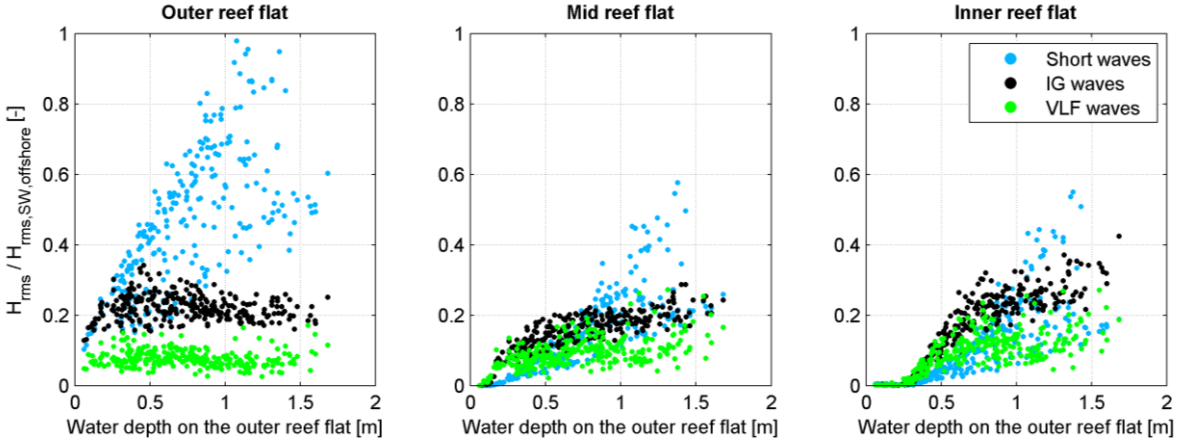

Figure 2.7 The burst-averaged short, infragravity (IG) and Very Low Frequency (VLF) root-mean-squared wave heights normalized by the offshore short wave height ($H_{rms,SW,offshore}$), plotted as a function of the water depth on the outer reef flat.

2.3.5 Water level variations over the reef

As discussed in section 1.1.1, the typical topography of an atoll reef has significant influence on the water level variations towards the shore. An important phenomenon is the setup of the water level on the reef flat due to breaking waves on the fore reef. For the data obtained at Kwajalein, burst-averaged mean water levels are computed for each pressure sensor and referenced to the mid reef reference level in the bathymetry (as in Figure 2.2). Figure 2.8 shows these mean water levels ($\overline{\eta}_i$) for the March event, where *i* refers to the instrument location. The mean water levels at the offshore and fore reef instruments are almost identical and show that the offshore tidal elevation varies from -1 m to +0.8 m. The pressure signals on the reef flat are strongly correlated with the offshore tidal elevations and there is a jump in the mean water level value with respect to the fore reef pressure sensor. This indicates there is a significant amount of setup present, especially during the peak waves around March 1st. This setup can be wave-induced and/or wind-induced. In this analysis it is assumed the contribution of the wind is negligible with respect to the wave contribution.

Furthermore, it is noticed the mean water level of the inner reef flat pressure sensor does not approach zero during low tide (e.g. low tides in the period from 02/25 up to 02/28 in Figure 2.8). This error is because the pressure sensor was placed in a little pool of water, hence the measured pressure will never approach zero. Data points with a value of $\overline{\eta}_{inner} < 0.20\ m$ are excluded from this analysis.

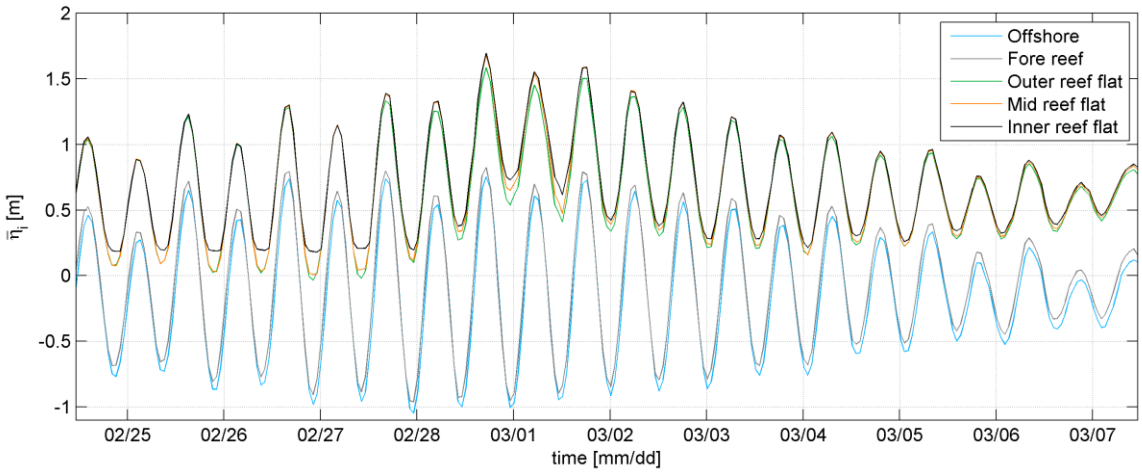

Figure 2.8 Time series of the burst-averaged mean water levels during the March event (i = offshore, fore reef, outer, mid or inner reef flat). $\overline{\eta}_i$ is relative to the reference level of the bathymetry.

Wave-induced setup is the mean water level variations resulting from wave forces due to wave breaking. Setup (η_{setup}) can be described by a horizontal momentum balance (Longuet-Higgins & Stewart, 1962),

$$\frac{dS_{xx}}{dx} + \rho g(\eta + h_0)\frac{d\eta}{dx} = 0 \qquad [2.6]$$

where S_{xx} is the cross-shore radiation stress, ρ the water density, g is the gravitational acceleration and h_0 is the still-water depth (in absence of waves). According to equation [2.6], a negative gradient in the cross-shore radiation stress (e.g. due to wave breaking) will be balanced with a positive gradient in the mean water level in cross-shore direction. Bottom friction can have an effect on the wave-induced setup on the reef flat and can be included in the horizontal momentum balance in equation [2.6]. However, Vetter et al. (2010) concluded the friction had a limited influence on the momentum balance because the reef flat of the Ipan reef is fairly smooth and featureless. As the reef flat at Roi-Namur has the same

characteristics, the friction contribution to the setup calculations is not considered in this analysis.

To calculate the wave-induced setup from the measured data at Kwajalein, the method of Vetter et al. (2010) is applied. The observed setup (η_{setup}) is calculated from the burst-averaged mean water levels ($\bar{\eta}_i$) and is referenced to the offshore AWAC ($\bar{\eta}_{offshore}$);

$$\eta_{setup,i} = \bar{\eta}_i - \bar{\eta}_{offshore} - h_0 \qquad [2.7]$$

where h_0 is the reference offset which accounts for the drifts over time for the pressure signals and it indicates the water level in absence of waves. As there are always waves present during the deployment period at Kwajalein, the reference offset is estimated using the same approach as Vetter et al. (2010). The reference offset is selected by conducting a regression analysis on the offshore wave height versus the mean water level difference between the offshore and reef flat instruments, so that η_{setup} = 0 when $H_{s,offshore}$ = *0*. This regression analysis and its results are presented in Figure 2.9. In the following setup calculations this reference offset (h_0) is set at a value of 0.33 m.

Vetter et al. (2010) also considers the effect of setdown on the offshore reference instrument at Ipan, Guam, which is located at a depth of ~8 m. The impact of setdown is assumed to be negligible in this study as the offshore AWAC used as reference is located at a depth of ~ 21 m.

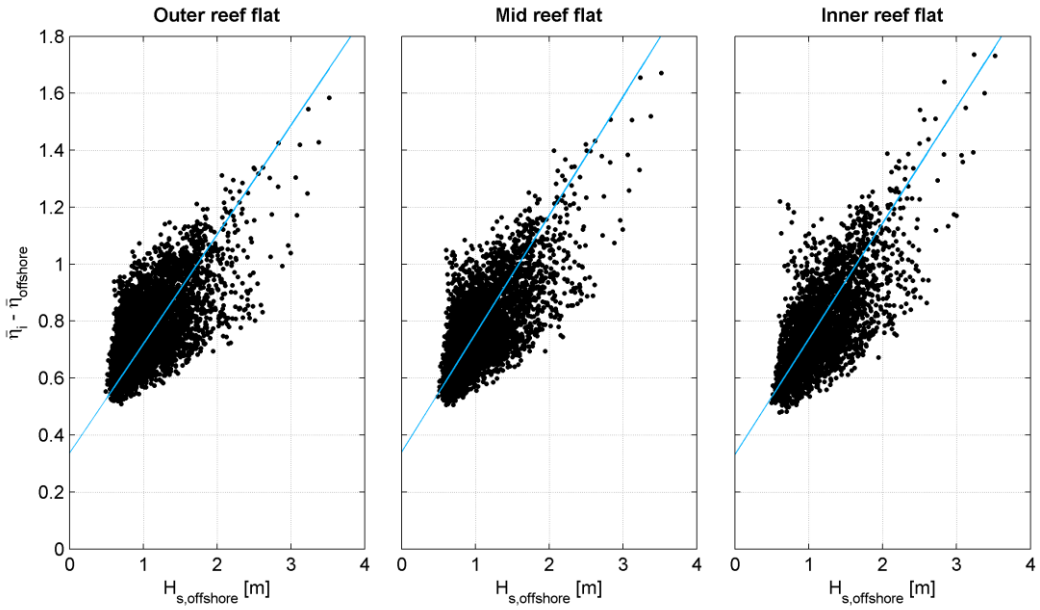

Figure 2.9 The burst-averaged mean water level difference between the offshore ($\bar{\eta}_{offshore}$) and reef flat instruments ($\bar{\eta}_i$) versus the offshore significant wave height. The regression line (blue line) gives estimation of reference offset when $H_{s,offshore}$ = 0. Data from the total deployment period is used in this figure.

Now the wave-induced setup can be calculated for each measurement location using equation [2.7] and the results are shown in Figure 2.10. The burst-averaged setup is plotted against the offshore significant wave height with its corresponding tidal elevation. At all measurement locations it shows an increasing setup as the incident wave height increases. This observation can be explained with equation [2.6]. As the wave height increases (and more wave energy is present) the cross-shore radiation stress will increase. The negative radiation stress gradient (e.g. due to wave breaking) will therefore be larger and is balanced with an equally larger positive gradient in mean water level. Hence the increasing setup values for increasing offshore wave height.

Additionally, setup exhibits an inverse dependence on tidal variations, with higher setup observed at low tide (and vice versa) for a certain offshore wave height (Figure 2.10). This phenomenon can be subscribed to the tidally dependent wave breaking on the fore reef slope (Becker et al., 2014 and Tait, 1972). During high tide the depth-limited wave breaking is weaker, resulting in a lower radiation stress gradient. As a consequence, according to the balance in equation [2.6], there is a lower positive gradient in mean water level and thus a lower setup. Similar correlations between setup and tidal elevations in reef environments were showed by Tait (1972) and Becker et al. (2014).

When comparing the measurement locations, it can be noticed there is an increase in setup for the highest setup values towards the shore. This can be caused by incomplete breaking which means that due to high water depths on the reef flat there is additional breaking of (small) waves on the reef flat.

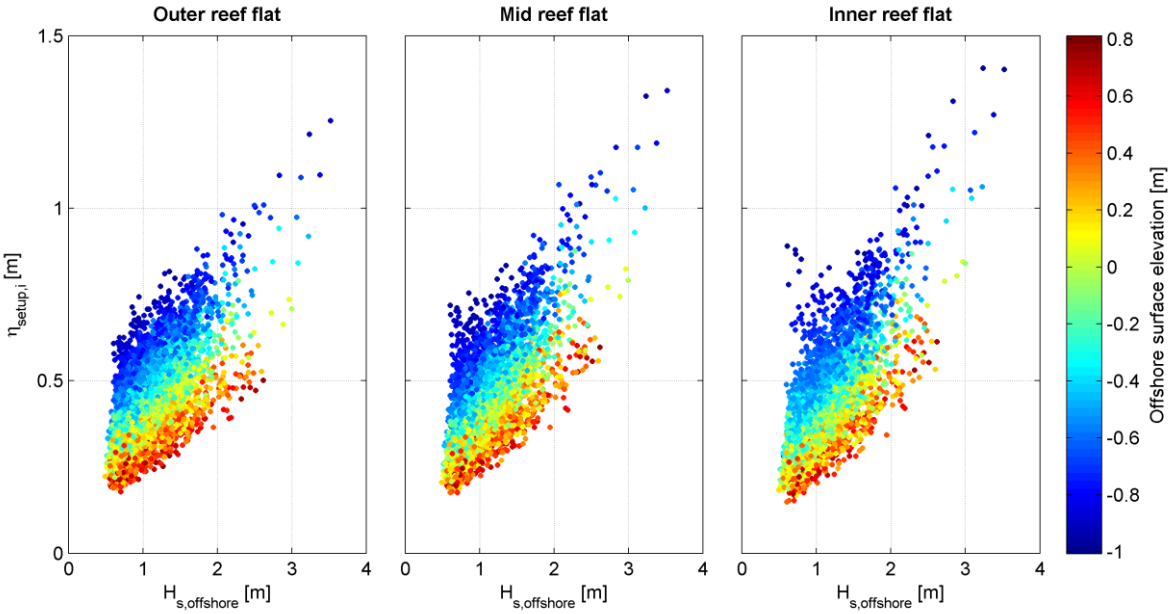

Figure 2.10 Setup on the reef flat versus the offshore significant wave height ($H_{s,offshore}$) colored with its corresponding offshore tidal elevation. Data from total deployment period is used in this figure.

2.4 Wave runup

As explained in section 1.1.2, wave runup is the vertical excursion of the water level at the shoreline and has been studied extensively for sandy beaches. However, knowledge on runup at beaches in reef environments is limited. During the field experiment at Kwajalein Atoll, runup data was collected by the digital time-lapse camera on the beach (Figure 2.2). Runup data is collected only for the period between 3 November 2013 and 17 December 2013. Just before the peak waves of the December event the camera failed due to the large wave forces. In this section the runup data obtained at Kwajalein Atoll is presented and analysed.

2.4.1 Methodology

The wave runup observations at Roi-Namur are photos of the beach in seaward direction taken every 30 minutes. At the beach five rocks at a fixed location are marked, as can be seen in the left photo in Figure 2.11. For each marked rock point the exact coordinates were determined and for each point its location along the bathymetry profile is defined (bottom panel in Figure 2.11). The rocks and their location on the bathymetry profile are used as reference points to give an indication of the maximum runup height. Each photo is analysed by picking the rock which is closest to the last wet point visible on the beach.

It is noted the maximum runup height is given here with respect to the reference level in the bathymetry (mid reef flat) and includes tidal elevation and setup. As a consequence it is from here on referred to as z_{max}, as defined in Figure 1.1.

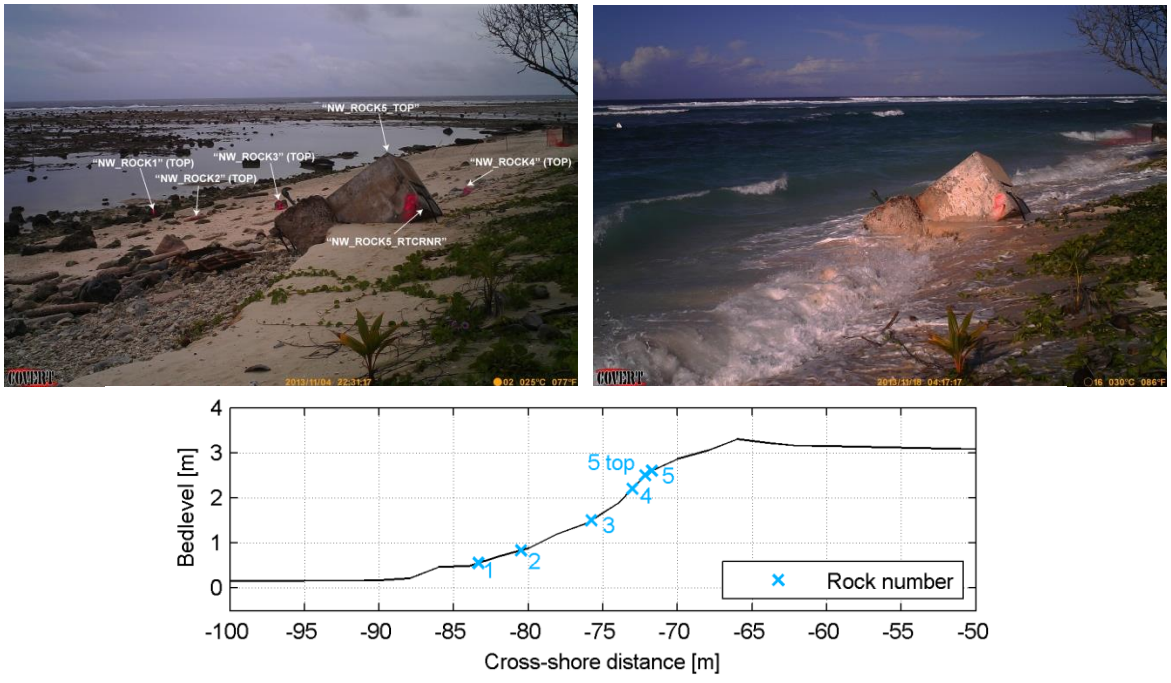

Figure 2.11 Rock locations on the beach (left photo) and the corresponding location on the bathymetry (bottom). The right photo is shows the observed extreme wave runup event.

2.4.2 Wave runup observations

The wave runup observations are shown in Figure 2.12, where z_{max} is plotted with the mean water levels and wave heights observed at the inner reef flat pressure sensor. As discussed in section 2.3.3, data points with a value of $\overline{\eta}_{inner} < 0.20$ m are excluded. In general, during high tide an additional vertical water level excursion with respect to the mean water level on the inner reef flat ($\overline{\eta}_{inner}$) is observed. This additional vertical water level excursion represents the maximum (infragravity and incident) swash excursion as $\overline{\eta}_{inner}$ includes the setup. During the higher water levels on the reef flat the wave heights increase, which corresponds with the results in Figure 2.7, and produces the higher z_{max} observations.

During the deployment period of the time-lapse camera there was a large wave runup event on 17 November 2013 at 16.17 pm, where the water level at the shoreline was outside the range of the photo. The corresponding photo is shown in Figure 2.11 in the right photo. The maximum vertical water level excursions, z_{max}, and the corresponding wave heights on the inner reef flat observed at Roi-Namur during this event are shown in Figure 2.12. The peak runup event is the result of a combination of high mean water level and high wave heights at the inner reef flat. At the peak moment, the short, IG and VLF wave heights are respectively 0.20 m, 0.40 m and 0.45 m.

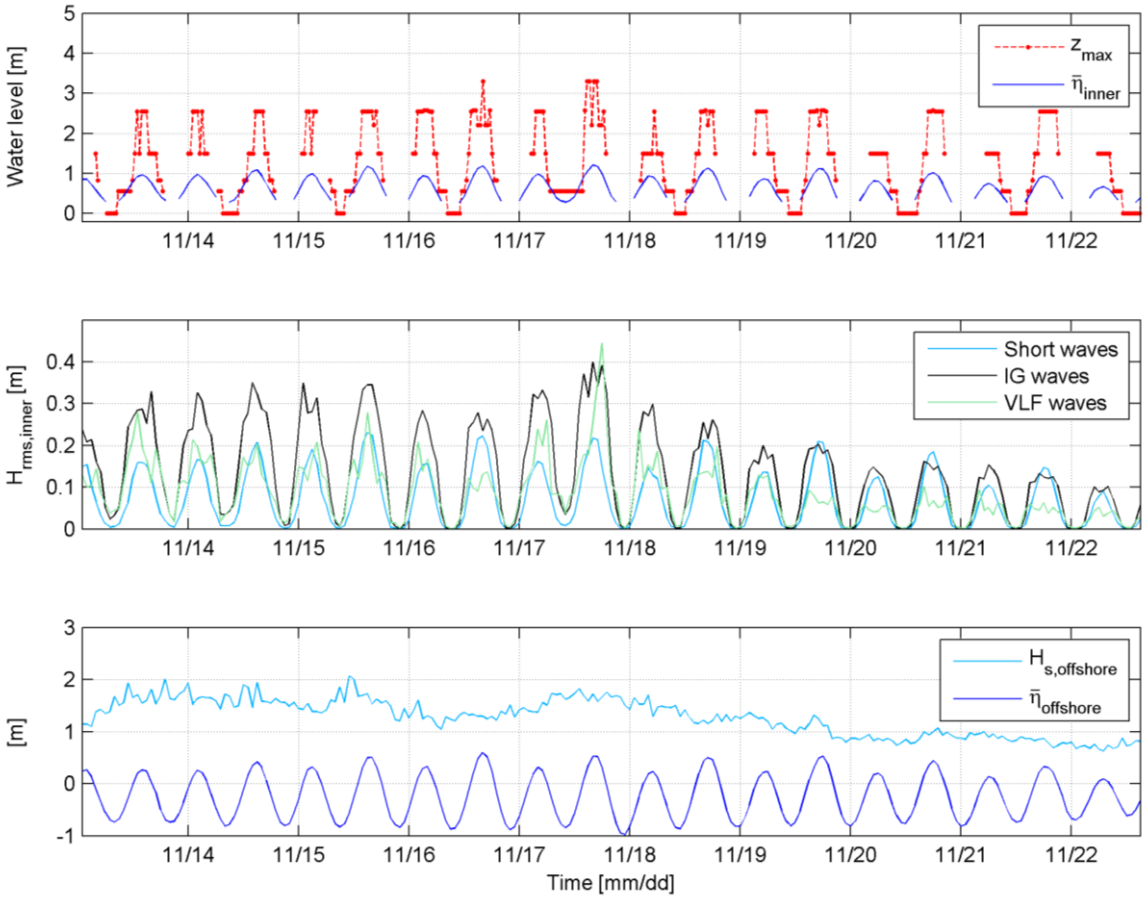

Figure 2.12 Wave runup observations (z_{max}) with its corresponding mean water levels (top) and wave heights (mid) on the inner reef flat. The corresponding offshore mean water levels and significant wave height are shown in the bottom panel.

2.5 Discussion

There is a difference in bottom roughness along the bathymetry profile (Figure 2.2). The steep fore reef slope has an irregular and rough topography and the reef flat has a relatively smoother surface. The effect of the reef flat roughness on the hydrodynamics on the reef flat is discussed in this chapter. It is expected the rough topography of the fore reef slope has an effect on the water levels and waves over the reef. Processes such as wave-induced setup and wave height transformations are primarily generated or changed on this section of the bathymetry profile. However, the influence of the fore reef roughness on the hydrodynamics across the reef is not quantified in this analysis.

The spectral evolution over the reef discussed in section 2.3.4 considers the total surface elevation signals and makes no distinction between onshore and offshore propagating waves. However, processes such as resonance and reflection of waves at the beach can have a significant contribution to the hydrodynamics on the reef (e.g. Péquignet et al., 2009 and Pomeroy et al., 2012). The amplitude of IG and VLF waves can be enhanced if the offshore forcing matches the resonant mode of the reef basin. Reflected waves at the beach can create a standing wave or can be topographically trapped due to refraction as an edge wave. Reflection of IG and VLF waves can be calculated by estimating the incoming and outgoing cross-shore energy fluxes. Incoming and outgoing energy fluxes cannot be calculated in this study, because no velocity data was measured at Roi-Namur. However, the main goal of this study is to understand the wave runup process at atoll reefs. The wave runup observations at Roi-Namur are the total vertical water level excursions, thus including the contributions by tidal elevation, setup, IG and incident swash.

An analysis as extensive as for the hydrodynamics across the reef is not possible for the runup observations because of the relatively large runup measurement rate. So no distinction can be made between the components infragravity and incident swash. However, looking at the context in which this study is carried out, the effect of sea level rise on inundation events at atoll islands, the extreme runup events are of interest. The swash motions on a small time scale are less important in this matter. The runup observations together with the hydrodynamic data over the reef can give a good indication of the processes causing the extreme runup events.

A final note is made on the accuracy of the wave runup observations. As the last wet points are visually determined and the measurement rate is relatively low, the observations are very sensitive to errors. For example, if there is a high wave runup just five minutes after a photo, the last wet point on the beach at the next photo can be changed due to drying of the beach.

2.6 Conclusions

Data obtained from the field study of the Roi-Namur Island at Kwajalein Atoll was analysed to provide insight into the relevant hydrodynamic processes. During the deployment period, 3 November 2013 to 13 April 2014, two energetic wave events occurred, referred to as the December and March event. The March event was the most energetic event, therefore this subset of the data was used for analysis.

The wave height evolution over the reef profile shows a general trend of increasing low frequency (IG and VLF) waves and decreasing high frequency (short) waves. From the analysis it was concluded that short wave energy dissipation was the result of both wave breaking and bottom friction, as observed in previous studies. IG and VLF waves were present on the reef flat and their magnitudes increased towards the shore. This suggests frictional dissipation plays a minor role in the IG and VLF wave height evolution across the reef due to the relatively smooth reef flat. Especially during the energetic March event the IG and VLF wave heights increase substantially and become dominant at the inner reef flat.

Additionally, the observations show that the short, IG and VLF wave heights on the reef flat were strongly determined by the local water depth, which is mainly the result of the offshore tidal variations. Comparing these results with the results at Ningaloo Reef by Pomeroy et al. (2012), it is suggested that the effect of frictional dissipation on the tidal modulation in IG wave heights is significant on the reef flat

The wave-induced setup on the reef flat increases as the offshore wave height increases and is reasonably constant across the reef flat. Furthermore, wave-induced setup is inversely correlated with the offshore tidal elevation due to depth-induced wave breaking on the fore reef slope. The water depth on the reef flat is therefore strongly affected by the tidal variations and the offshore wave height, and consequently affects the (short, IG and VLF) wave height on the reef flat.

Runup observations were collected for the period between 3 November 2013 and 17 December 2013 and included one extreme runup event. This is the result of a high mean water level on the reef flat and high wave heights at the inner reef flat. As the water depth increases on the reef flat, the wave heights at the shoreline increase. This results in higher maximum vertical water level excursion, z_{max}, observations.

3 The XBeach model

3.1 Introduction

XBeach is a two-dimensional depth-averaged process-based numerical model for wave propagation, flow, sediment transport and morphological changes in the nearshore coastal area. XBeach has been successfully applied to predict the nearshore response during storm and hurricane conditions including processes like overwash, dune erosion and breaching of barrier islands and dunes (e.g. McCall et al., 2010; Roelvink et al., 2009). More recently, XBeach has been used to model reef environments (Bodde, 2013; Pomeroy et al., 2012; van Dongeren et al., 2013) and proved to give a good prediction of the hydrodynamic processes related to a reef environment.

In this chapter a description of the most important physical processes and model formulations is given. The present study focusses on the one-dimensional hydrodynamics associated with atoll reef systems. Consequently, the morphology and sediment transport module of XBeach are not activated and will not be elaborated further on in this chapter.

In section 3.2 a brief description of the relevant model formulations in XBeach is given, where a distinction is made into the hydrostatic and non-hydrostatic model version of XBeach. Section 3.3 elaborates on the applicability of XBeach for the particular case of a reef environment.

3.2 XBeach model description

In this section a description of the XBeach model is given, where a differentiation is made in the hydrostatic and non-hydrostatic model. Only the parts of the model which are relevant for this thesis are discussed here. For a more complete description of the XBeach model reference is made to Roelvink et al. (2009).

3.2.1 Hydrostatic model

XBeach solves for water level variations up to the scale of long (infragravity) waves using the depth averaged non-linear shallow water (NLSW) equations. The NLSW-equations are coupled to a wave action balance, in which the variations of wave energy due to the short wave groups are solved. The radiation stress gradients derived from these variations in the short wave groups result in a wave force that is included in the shallow water equations, and generates long waves and setup of the water level within the model.

The effect of bottom friction on the short wave dissipation proved to be significant for reef environments (Lowe et al., 2005). To take this dissipation into account an additional term related to this friction (D_f) is added to the wave action balance;

$$\frac{\partial A}{\partial t}+\frac{\partial c_x A}{\partial x}+\frac{\partial c_y A}{\partial y}+\frac{\partial c_\theta A}{\partial \theta}=-\frac{D_b}{\sigma}-\frac{D_f}{\sigma} \qquad [3.1]$$

where c represents the propagation velocity in the direction of the subscript x (cross-shore), y (alongshore) and θ (directional), D_b is the dissipation by wave breaking and σ is the representative radian wave frequency. A is the wave action and represents the wave energy density in each directional bin for its representative radian wave frequency ($A = E/\sigma$). The bottom friction dissipation term (D_f) in the wave action balance is calculated as (van Dongeren et al., 2013):

$$D_f=\frac{2}{3}\rho\pi f_w\left(\frac{\pi H_{rms}}{T_{m01}\sinh kh}\right)^3 \qquad [3.2]$$

where ρ is the water density, f_w is the short wave friction coefficient, T_{m01} is the mean period, k the wave number and h represents the water depth. H_{rms} is the root-mean-squared wave height and is calculated from the wave energy.

In the wave action balance (equation [3.1]), D_b represents the wave energy dissipation by wave breaking and is used as a source term for the roller energy balance. The roller energy balance captures the process of roller formation and propagation and adds the variation in roller-induced radiation stress to the wave force. The energy dissipation due to depth-limited wave breaking is modelled according to Roelvink (1993a):

$$D_b=2\frac{\alpha}{T_{rep}}Q_b E_w\frac{H_{rms}}{h} \qquad [3.3]$$

where α is a calibration coefficient (O(1)), T_{rep} is the representative wave period, Q_b a probability function and E_w the wave energy. The value of D_b strongly depends on the ratio H_{rms}/h, which determines the point where wave breaking occurs. This is called the breaking parameter ($\gamma_b = H_{rms}/h$) and the default value in XBeach is set at 0.55.

The mean currents and long wave motions are solved within the depth averaged momentum and continuity equations. The friction associated with mean currents and long waves is included in the shallow water equations by the bed shear stress (τ). Using the approach of Ruessink et al. (2001) this bed shear stress is calculated with;

$$\tau = c_f \rho U_E \sqrt{(1.16 u_{rms})^2 + (U_E^2 + V_E^2)} \quad [3.4]$$

where c_f is the friction coefficient associated with both mean currents and long waves, U_E and V_E are the local Eulerian flow velocities in the direction of respectively x (cross-shore) and y (alongshore) and u_{rms} is the local orbital velocity.

3.2.2 Non-hydrostatic model

A more complete way to simulate wave-dynamics can be achieved by applying phase-resolving models like Boussinesq or non-hydrostatic models. Such models resolve the wave field on the scale of individual waves and are able to model the non-linear wave field evolution and dispersion. A downside to the Boussinesq models is a separate breaking model is generally needed to capture wave breaking. Stelling and Zijlema (2003) showed that non-hydrostatic models can be more efficient by constructing an edge based finite difference scheme in the vertical. Additionally, Zijlema and Stelling (2008) showed wave breaking can be accurately modelled in a non-hydrostatic model without using a separate breaking model.

A non-hydrostatic module was implemented into the existing XBeach model by Smit (2008) using a numerical scheme based on Stelling and Zijlema (2003) and Zijlema and Stelling (2008). XBeach is depth-averaged and therefore the non-hydrostatic module has one vertical computational layer, in contrast to other non-hydrostatic models like SWASH (Zijlema, Stelling, & Smit, 2011).

The main advantage of the non-hydrostatic model is that it is more accurate compared to the hydrostatic model as it solves both high and low frequency motions on the individual wave scale. As a consequence, it is a more reliable way to solve the individual wave breaking process and the short wave runup on the beach. However, the grid resolution of the model has to be significantly smaller for the non-hydrostatic module, resulting not only in a substantial increase in grid cells, and thus computational time.

3.3 XBeach model applicability

Whether the XBeach model is suitable for modelling the hydrodynamics and runup on an atoll reef is determined by its capability to represent the relevant processes present in reef environments. As discussed in section 1.1, dominant hydrodynamic processes associated with reef environments are;

- Dissipation of wave energy due to wave breaking and bottom friction;
- Wave-induced water level setup on the reef flat;
- Presence of low frequency wave motions;
- Wave runup at the beach.

Hydrostatic model

The transformation and propagation of the waves across the reef are highly depending on wave energy dissipation due to bottom friction and wave breaking (e.g. Young (1989); Lee and Black (1978); Lowe (2005)). In the hydrostatic model of XBeach the shallow water equations are forced by the wave action balance, and fully resolve for water level motions and runup up to the long wave scale. This wave action balance captures wave energy dissipation by wave breaking (D_b) and bottom friction (D_f) as can be seen in equation [3.1]. The higher bottom roughness characterizing the reef environments can be simulated with XBeach by locally increasing the short wave friction coefficient (f_w) and current friction coefficient (c_f), and is implemented in the model according to equations [3.2] and [3.4]. Energy dissipation due to wave breaking is taken into account using equation [3.3].

In section 2.3 it is shown wave-induced setup and long wave motions dominate the hydrodynamics on the reef flat at Roi-Namur, which corresponds with previous studies (e.g. Pomeroy et al., 2012; Vetter et al., 2010). Water level setup and long waves are captured in the hydrostatic model of XBeach by the variations in radiation stresses from the short wave groups which lead to a wave force in the shallow water equations.

In general, good results of using the hydrostatic model of XBeach in a reef environment were reported by e.g. van Dongeren et al. (2013). They all accurately reproduced the water levels, infragravity and short wave heights by calibrating the friction coefficients (f_w and c_f). It was also shown that the model gives a good prediction of the infragravity waves on a fringing coral reef.

The knowledge of wave runup on coasts fronted by a reef is limited, but is an important process to model correctly in order to simulate the inundation events at atoll reefs. Wave runup can be modelled with XBeach by detecting the shoreward-most wet point at each output time step. Stockdon et al. (2014) evaluated the wave runup predictions of the hydrostatic version of XBeach (for both one- and two-dimensional spatial domain) including storm conditions. Their results suggested XBeach can be used to numerically simulate wave runup in predictive mode.

The XBeach hydrostatic model does not resolve high frequency motions explicitly but does compute the wave-induced setup and low frequency wave motions which means the simulated runup will not include the incident swash motions (Stockdon et al., 2014). However, the lower frequency motions and setup are expected to dominate the shallow reef flat, so the hydrostatic version of XBeach is expected to be a suitable tool to model wave runup on an atoll reef.

Non-hydrostatic model
Although the non-hydrostatic model of XBeach has not been applied yet in reef environments, it is expected to simulate the hydrodynamic processes more accurately as it resolves water level motions on the individual wave scale (incident-band and infragravity motions). Thereby both high and low frequency motions are resolved within the model so the computed swash motions include both its infragravity and incident components.

In this study the XBeach non-hydrostatic model is preferred over other non-hydrostatic models, e.g. SWASH. SWASH could be more accurate because multiple vertical layers can be applied in the model. However, a better comparison of hydrostatic and non-hydrostatic results can be made if the XBeach non-hydrostatic model is used. Additionally, the model setup can be almost identical, which will reduce time setting up the model.

In section 2.3.4 it is shown the short wave heights on the reef flat strongly depends on the water depth on the reef flat. Therefore, there can be a significant contribution by the incident swash during storm conditions, since high energy wave conditions can result in a relatively large wave-induced setup on the reef flat. By comparing the results of the hydrostatic and non-hydrostatic version of XBeach the relative importance of short waves on the total wave runup can be investigated.

4 Model results

4.1 Introduction

In this chapter the capability of the XBeach model to simulate the wave runup at the Kwajalein atoll reef is tested. In order to simulate the wave runup correctly, the hydrodynamics across the reef must first be properly reproduced by the model. The data on water levels, waves and wave runup measured on the Roi-Namur island at the Kwajalein Atoll (Chapter 2), is used to calibrate and validate the model.

Three major events are selected from the Kwajalein dataset and used for model calibration and validation. In Figure 4.1 the offshore sea states of the total deployment period is shown with the three major events highlighted. The two high energy wave events in March (red line) and December (green line) are used for respectively calibration and validation of the modelled hydrodynamics across the reef. First, the model is calibrated with the data of the March event. The required optimum friction coefficient values are identified to reproduce the key hydrodynamic processes across the reef. Subsequently, the model is validated by imposing different forcing conditions on the calibrated model configuration. The December event is used to validate the model. The orange line denotes the extreme wave runup event (presented in section 2.4.2) and is used for validation of the infragravity and incident wave runup.

In this chapter first the model setup for the XBeach simulations is presented in section 4.2. Next, the results on reef hydrodynamics using the XBeach hydrostatic model are discussed in section 4.3, followed by the infragravity wave runup in section 4.4. Subsequently, the relative importance of the incident wave runup is investigated using the XBeach non-hydrostatic model in section 4.5. Finally, after discussing the main model results (section 4.6), the main conclusions are presented in section 4.7.

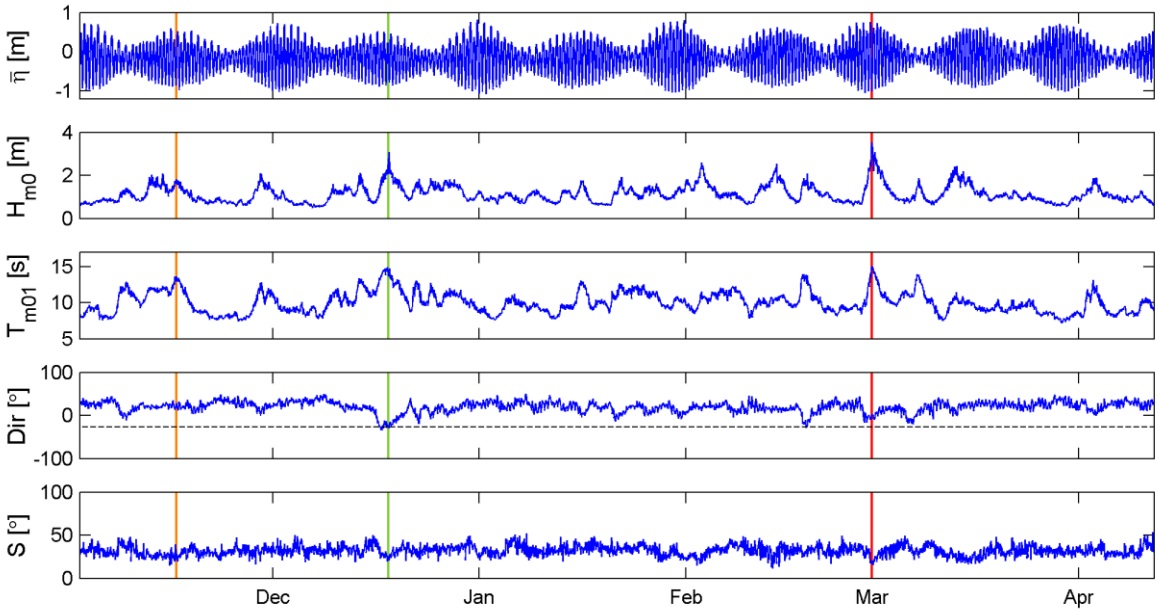

Figure 4.1 Burst-averaged offshore sea states for the total deployment period. The orange, green and red line represents respectively the extreme wave runup event, the December event and the March event.

4.2 Model setup

The offshore tidal elevation and wave conditions in Figure 4.1 are applied to the offshore boundary of the model domain. From the wave conditions (wave height, wave period, mean direction and directional spreading) a sequence of hourly varying JONSWAP spectra are created. From these spectra XBeach generates time series for the short wave energy and the bound long wave with an approach described by van Dongeren et al. (2003). The measured offshore water level is averaged per hourly burst of data and subsequently used as initial surface elevations at the offshore model boundary.

The measured cross-shore profile of Roi-Namur (Figure 2.2) is used as bathymetric profile in the simulations. The numerical grid size is constant for all simulations and varies from dx = 20 m offshore to dx = 1 m in shoreward direction.

At the offshore boundary a weakly-reflective boundary condition is applied where outgoing waves and currents can pass through to deep sea with minimal reflection. A no flux/wall boundary is applied at the shoreward model boundary. At the lateral boundaries a Neumann boundary condition is used, in which there are no gradients in surface elevation and velocities in alongshore direction.

The numerically computed wave runup is extracted by inserting a virtual runup gauge in XBeach. The wave runup variations are detected in XBeach by determining the shoreward-most wet point at a certain threshold depth. This threshold depth can influence the magnitude of the simulated swash measurements, analogous to field measurements (e.g. Holland (1995) and Raubenheimer et al. (1995)). The runup tongue contains a very thin layer of water which cannot be measured accurately. Due to the shape of the runup tongue the measured vertical excursion will decrease as the sensor elevation increases. It is suggested by TAW (2002) the runup level is determined by the level at which the runup tongue is less than 2 cm thick. Therefore, the threshold depth in the XBeach simulations is set at 2 cm.

4.3 Hydrodynamics across the reef

In this section the results of the XBeach model performance on reproducing the hydrodynamics across the reef is presented. The simulations for both calibration (section 4.3.1) and validation (section 4.3.2) have a duration of 2 days (48 hours) in order to evaluate the model for different wave conditions and tidal elevations.

The model output consists of time series of the short wave height and water level for each measurement location. The water levels include tidal elevation, wave-induced setup and infragravity (IG) wave motions. To compare the model output with the measurements at Roi-Namur, the mean water levels, short and IG wave heights are calculated for each hour bin of model output. To evaluate the calibration and validation results with respect to the measurements, the bias and scatter index (SCI) are calculated for each simulation. In equations [4.1] and [4.2] these statistical measures as defined by Roelvink et al. (2009) are presented. The predictive skill of a model can be determined by calculating the bias and SCI. The SCI measures the scatter between modelled and measured variables. The error is normalized with the maximum of the root-mean-square of the data and the absolute value of the mean of the data.

$$bias = \frac{1}{n}\sum_{i=1}^{n}(X^{i}_{modelled} - X^{i}_{measured}) \qquad [4.1]$$

$$SCI = \frac{\sqrt{\frac{1}{n}\sum_{i=1}^{n}(X^{i}_{modelled} - X^{i}_{measured})^{2}}}{\frac{1}{n}\sum_{i=1}^{n}X^{i}_{measured}} \qquad [4.2]$$

where n is the number of data points and X^{i} is the modelled or measured variable.

4.3.1 Calibration

The main purpose of the calibration is to identify the values for the friction coefficients (f_w and c_f) which optimize the results of XBeach. The calibration process consisted of two phases. First, the simulations were conducted for v and a constant current friction coefficient (c_f = 0.1, van Dongeren et al. (2013)). Subsequently, a varying c_f was applied while the f_w was kept constant at the calibrated value. From the results of these simulations it was observed the c_f coefficient resulted in inconsistent variations in water levels and IG wave heights across the reef. As discussed in section 2.5, it is expected that the difference in bottom roughness along the bathymetric profile has an influence on the hydrodynamics across the reef. Therefore, a spatially varying c_f was applied in the model in the second calibration phase. The model is calibrated using three (spatially varying) friction coefficients;

- short wave friction (f_w)
- current friction for the fore reef ($c_{f,fore}$), section between -520 m and -350 m in Figure 2.2
- current friction for the reef flat ($c_{f,flat}$), section between -350 m and 0 m in Figure 2.2

The current friction coefficient for the fore reef is applied offshore of the reef crest (i.e. point were the fore reef converts into the reef flat). Shoreward of the reef crest the current friction coefficient for the reef flat is implemented. As the fore reef has a more irregular and rough topography with respect to the reef flat at Roi-Namur, $c_{f,fore} > c_{f,flat}$.

The best result is achieved with the friction coefficients as presented in Table 4.1, and is referred to as 'simulation C1'. The optimum friction coefficient values found for the Roi-Namur study site are lower with respect to the friction coefficients applied in the Ningaloo Reef XBeach model (van Dongeren et al., 2013), i.e. f_w = 0.6 and c_f = 0.1. This is consistent with the expectations, as the Roi-Namur reef flat has a relatively smooth bottom topography.

Table 4.1 The optimum friction coefficients resulting from the calibration.

Simulation	f_w *[-]*	$c_{f,fore}$ *[-]*	$c_{f,flat}$ *[-]*
C1	0.15	0.4	0.01

The results of simulation C1 are presented in Figure 4.2 and Figure 4.3, by respectively a scatterplot and the time series. In both figures the modelled and measured results for the mean water level, long and short wave heights (vertically outlined) are compared for each measurement location across the reef (horizontally outlined). In addition, the statistical measures of simulation C1 are shown in Figure 4.4.

For simulation C1 in general good agreement is observed between model results and measurements, as can be seen in Figure 4.2, Figure 4.3 and Figure 4.4. Inspecting Figure 4.2, especially the three pressure sensors on the reef flat show a strong correlation for the model predictions and measurements. The short wave height on the fore reef and outer reef flat is underestimated (bias = -0.25 - -0.14m, SCI = 0.17 – 0.25), which can be explained by the difference in the location of the offshore AWAC at Roi-Namur and in the model. A small increase in short wave height from the offshore to the fore reef location was noticed in the measurements (section 2.3.4), probably due to processes such as refraction. In the model results the short wave height remains constant over this area (Figure 4.3), as the offshore measurement location is in line with the fore reef measurement location and depth-induced wave energy dissipation is negligible.

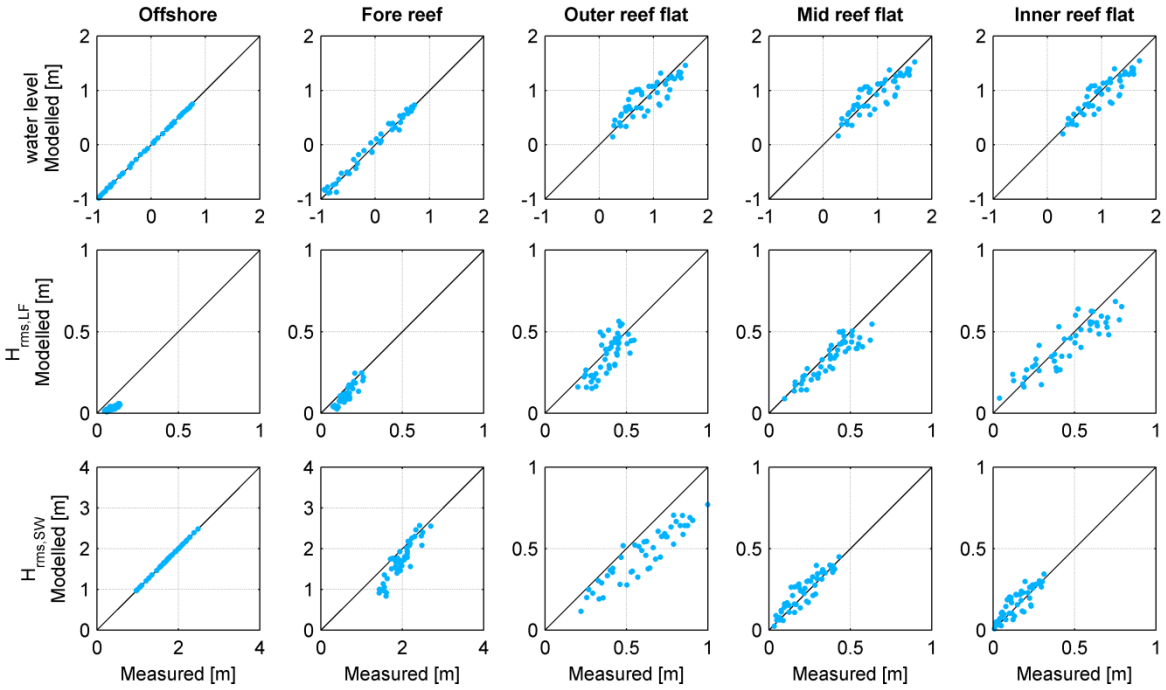

Figure 4.2 Results of the calibration simulation with the optimum friction coefficients. Scatterplot of the modelled and measured burst-averaged mean water level, long and short wave height (rows) for each instrument (columns).

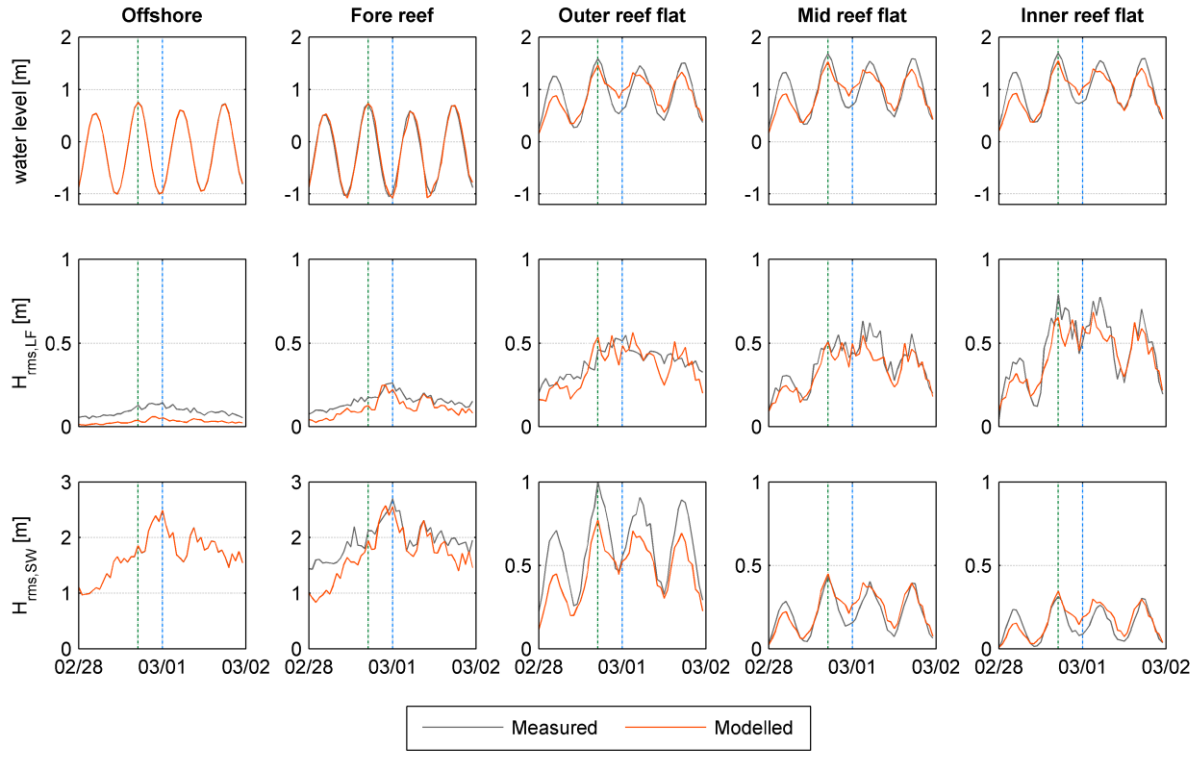

Figure 4.3 Results of the calibration simulation with the optimum friction coefficients. Time series of the modelled (orange) and measured (grey) burst-averaged mean water level, long and short wave height (rows) for each instrument (columns).The blue and green line denotes the characteristic moments presented in Figure 4.5.

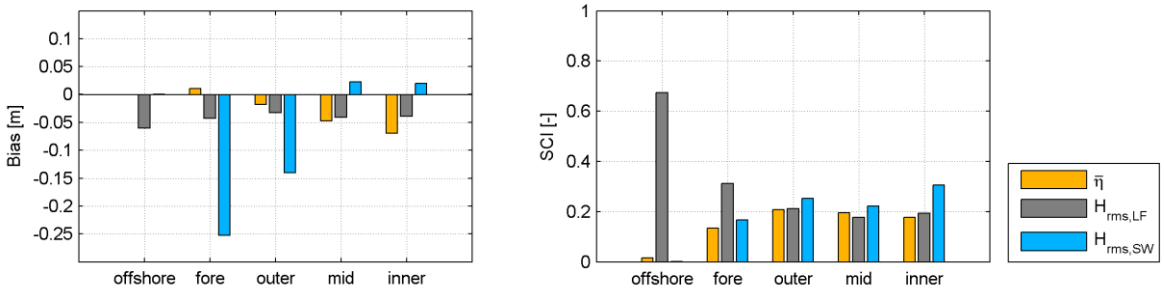

Figure 4.4 Bias and scatter index for simulation C1.

The optimum model configuration of simulation C1 is now used to provide insight into the simulated key hydrodynamic processes. The spatial distribution of the mean water levels, long and short wave height along the cross-section of the reef for two characteristic moments in simulation C1 representing a high and low tide (i.e. the blue and green line in Figure 4.3) are shown in Figure 4.5. The blue points and lines represent the hydrodynamics during low tide and are during the most energetic waves in the March event. The green points and lines represent the hydrodynamics during the high tide six hours before the most energetic wave event.

For the high tide the modelled mean water levels in Figure 4.5 are found to agree well with the measured values. However, during the peak wave event XBeach overestimates the water level on the reef flat. This is probably because the location of wave breaking cannot be accurately predicted by XBeach. As wave-induced setup is strongly dependent on the water depth at wave breaking (equation [2.6]), an inaccurate location of wave breaking can result in errors in the reef flat water levels, since the bed is relatively steep. Additionally, there is a significant wave setup on the reef visible for the peak wave event (and low tide) compared to the results during high tide. The relatively strong wave setup is due to the higher offshore wave heights and tidally-dependent depth-induced wave breaking. This is consistent with the phenomena observed in the data analysis of the water level variations in section 2.3.3.

The modelled long wave heights ($H_{rms,LF}$) in Figure 4.5show there is an increase in long wave height towards the shore, which is consistent with the Kwajalein measurements. For the peak event during low tide, $H_{rms,LF}$ is overestimated by XBeach on the reef flat as a result of the overestimated setup on the reef flat. Furthermore, the model results show there is shoaling of the long waves along the fore reef, which is strongest during the peak wave event.

The short wave heights across the reef are well reproduced by the model. First, there is some shoaling of the short waves towards the fore reef point. Subsequently, waves are breaking on the fore reef slope which results in the rapid decrease in short wave height on the reef flat. Additionally, the model also reproduces the tidal dependency of the short wave height on the reef flat. Although the offshore wave heights are higher during low tide (peak wave event), the remaining short wave height on the reef flat is smaller. During high tide the dissipation of wave energy is smaller than during low tide. This tidal dependency can be related to the allowable height of waves as the water depth varies on the reef flat and is consistent with the results presented in Figure 2.7.

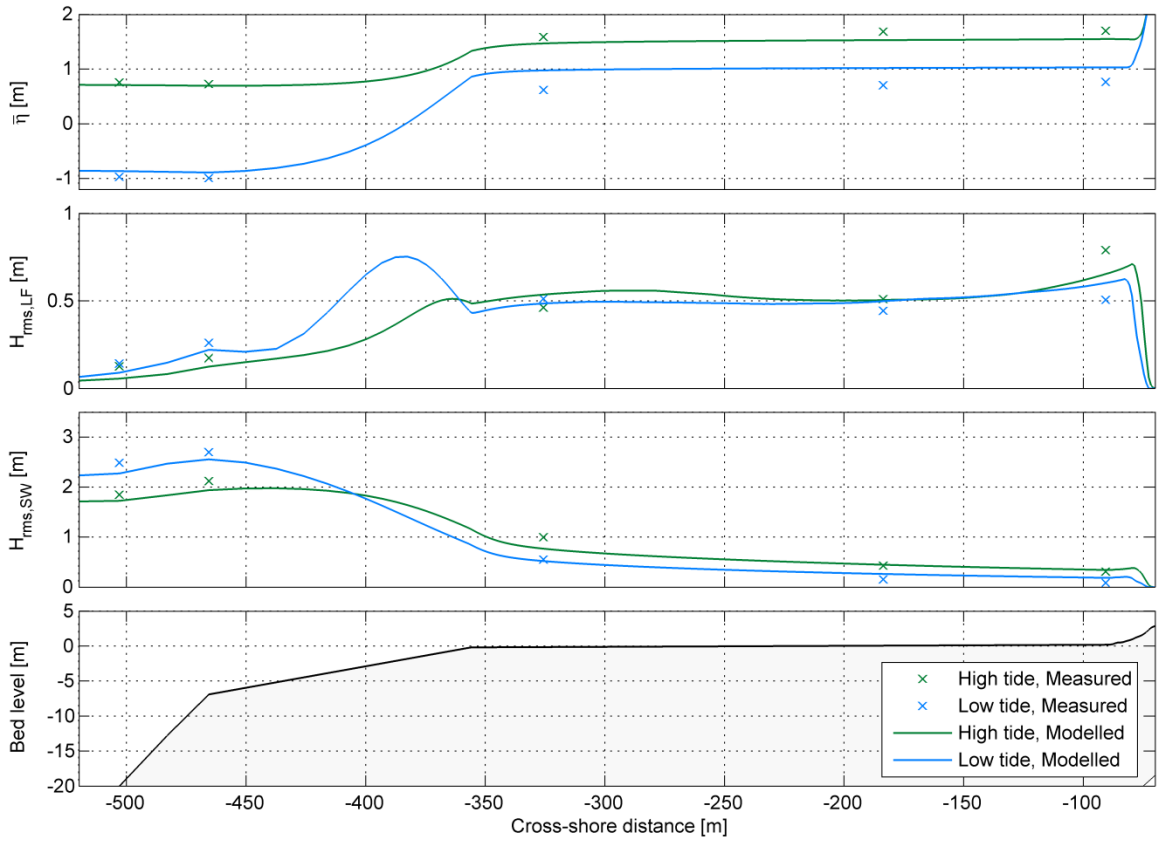

Figure 4.5 Cross-section of the XBeach results (solid line) and the measured values ('x') for two moments in the C1 simulation. Blue is during the peak wave event, green 6 hours before the peak event.

To show the sensitivity of the model to the friction coefficients on the key hydrodynamic processes, simulations C2, C3 and C4 are plotted with the best-fit simulation C1 in Figure 4.6. The combinations of friction coefficients for each simulation are shown in Table 4.2. The statistical measures of simulation C2, C3 and C4 are attached in Appendix A.

In simulation C2 the $c_{f,fore}$ is lowered with respect to simulation C1. Comparing both simulations in Figure 4.6, in general a small decrease in magnitude for each hydrodynamic parameter can be noticed on the reef flat locations. Adjustment in the flow friction coefficient, c_f will generally affect the computed mean currents and long wave motions (section 3.2.1). In this case, lowering of the c_f on the fore reef resulted in a smaller wave-induced setup and hence a decrease of the mean water levels on the reef flat. Due to the relatively small water depths on the reef flat, the long and short wave heights also decrease. This corresponds with the depth-dependent wave heights on the reef flat as observed in de data analysis in section 2.3.4.

In simulation C3 the current friction coefficient on the reef flat ($c_{f,flat}$) is increased compared to simulation C1. In Figure 4.6 the effect of this adjustment is clearly visible for the long wave height on the mid and inner reef flat. The locally increased friction coefficient on the reef flat causes more dissipation of the long wave motions and thus a decreasing long wave height. This supports the hypothesis in section 2.3.3 that the relatively smooth reef flat resulted in an increasing IG wave height towards the shore (instead of a decreasing IG wave height observed at Ningaloo reef by Pomeroy et al. (2012)).

Finally, the short wave friction coefficient (f_w) is adapted in simulation C4 with respect to simulation C1. An increased short wave friction coefficient generates lower short wave heights on the reef flat, as can be seen in Figure 4.6.

Table 4.2 Friction coefficients applied in simulation C1 to C4.

Simulation	f_w [-]	$c_{f,fore}$ [-]	$c_{f,flat}$ [-]
C1	0.15	0.4	0.01
C2	0.15	0.2	0.01
C3	0.15	0.4	0.05
C4	0.3	0.4	0.01

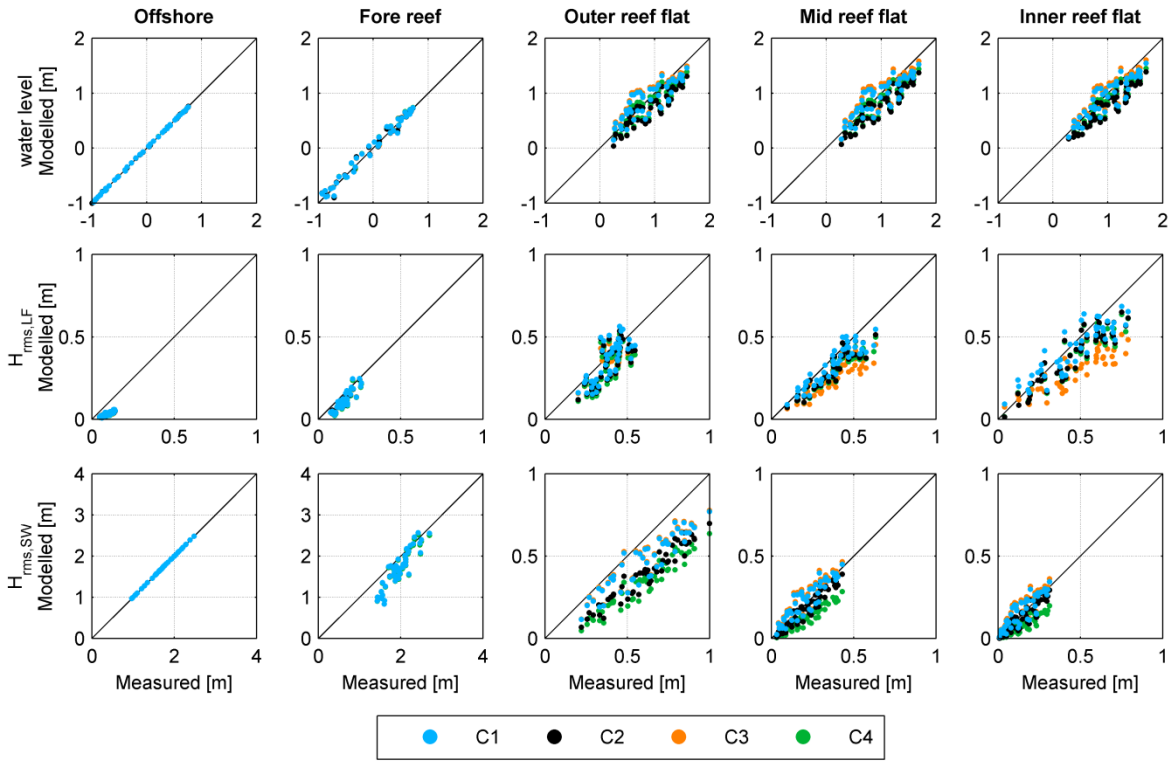

Figure 4.6 The modelled and measured burst-averaged mean water level, long and short wave height (rows) for each instrument (columns). The coloured dots represent simulation C1 to C4, with its corresponding friction coefficients in Table 4.2.

4.3.2 Validation

The calibrated friction coefficient values (Table 4.3) are now used to validate the model using the December event. Similar to the calibration in the previous section, the modelled and measured results are compared for the mean water level, long and short wave heights. The results are presented in Figure 4.8 and Figure 4.9. In both figures the modelled and measured results for the mean water level, long and short wave heights (rows) are compared for each measurement location across the reef (columns).The statistical measures of the validation simulation V1 are presented in Figure 4.7.

Table 4.3 Friction coefficients applied for validation

Simulation	f_w [-]	$c_{f\ fore}$ [-]	$c_{f\ reef\ flat}$ [-]
V1	0.15	0.4	0.01

In general the results from the validation simulation are very similar to the calibrated results of simulation C1. Again, there is an underestimation of the modelled short wave height on the fore reef and the outer reef flat. Additionally, there is more variability in the modelled long wave height at the offshore and fore reef location with respect to the measurements.

The similarity of the C1 and V1 simulations is also represented in the statistical measures in Figure 4.4 and Figure 4.7. There is a small increase in the bias and SCI for the long wave height over the reef flat for the V1 simulation. However, the statistical measures for the short wave height and water levels in general are even better with respect to the calibrated simulation.

From this validation it can be concluded the optimum friction coefficients obtained in the calibration are performing very well for a different energetic wave event at Roi-Namur.

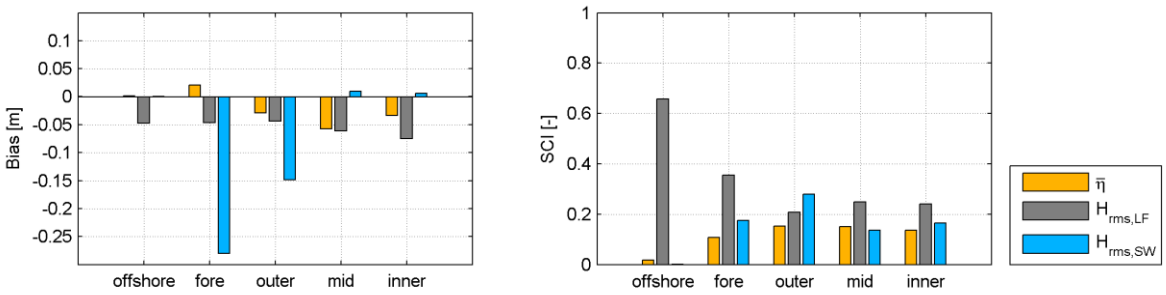

Figure 4.7 Bias and scatter index for the validation simulation V1.

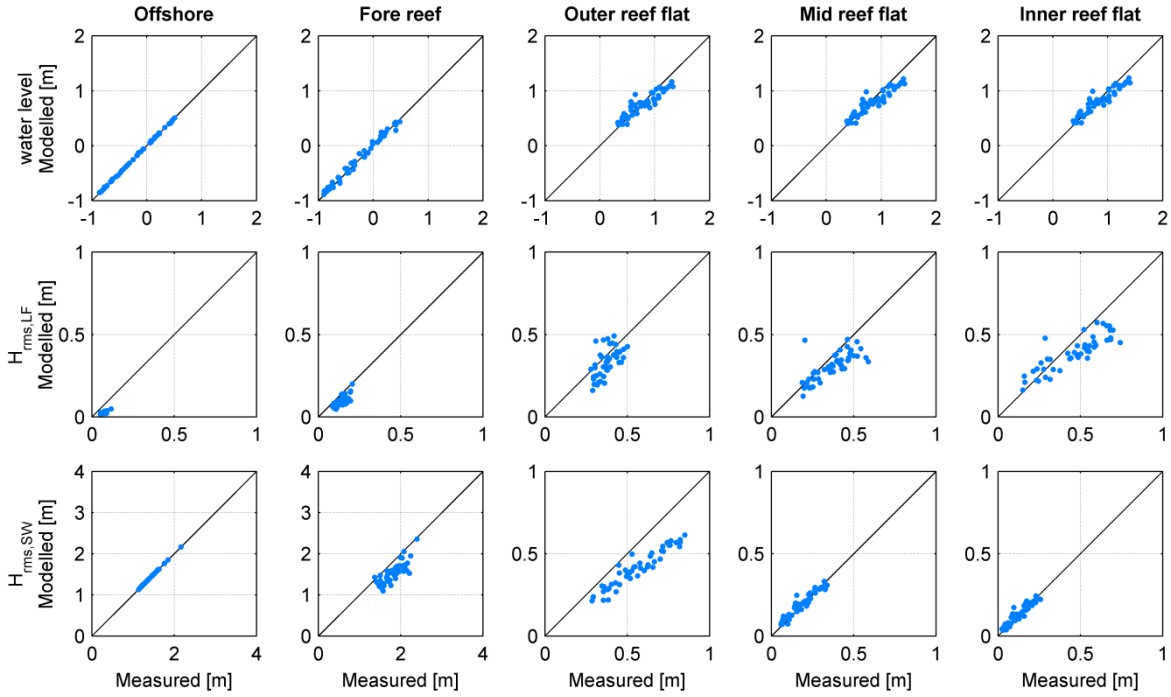

Figure 4.8 Validation simulation (V1) with the December event. The modelled and measured burst-averaged mean water level, long and short wave height (rows) for each instrument (columns).

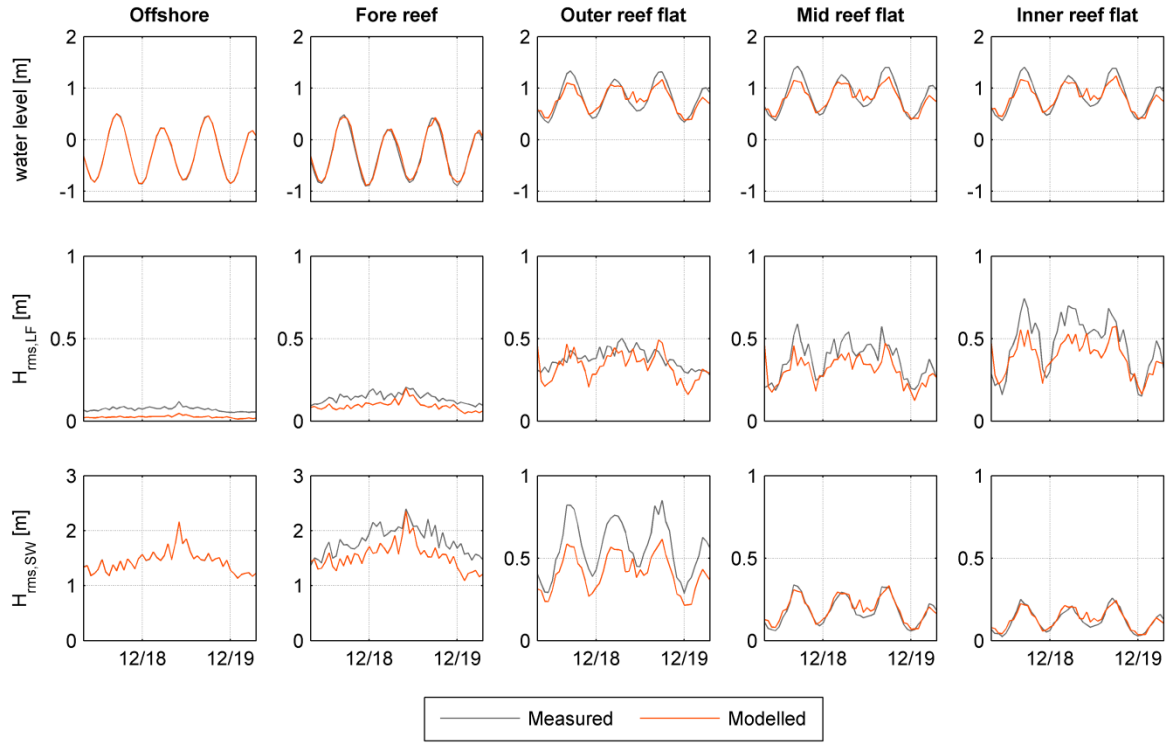

Figure 4.9 Simulation V1 with the December event. Time series of the modelled (orange) and measured (grey) burst-averaged mean water level, long and short wave height (rows) for each instrument (columns).

4.4 Infragravity wave runup

In the previous section it is shown that the hydrodynamics across the reef can be well reproduced by the XBeach hydrostatic model by using default settings as much as possible while calibrating on the friction coefficients. The calibrated settings were used to simulate infragravity wave runup at the Kwajalein Atoll. The model results are validated with the peak wave runup event that occurred in November, which was analysed in section 2.4.2.

Two moments with the highest wave runup observed in the measurements were selected for validation; event ‘a’ and ‘b’, as can be seen in the bottom panel in Figure 4.10. For each event a one hour simulation is conducted with its corresponding offshore tidal and wave conditions. The simulated runup is a continuous time series of the most shoreward-located wet grid point. In order to compare it with the Kwajalein measurements, the maximum runup value of the time series is determined (z_{max}).

The results of both simulations are presented in the two top panels in Figure 4.10. The red colour represents the wave runup at the beach and it is evident the modelled z_{max} is significantly lower than the observed z_{max}. This is in contrast with the modelled hydrodynamics across the reef. The short and long wave heights across the reef are in very good agreement with the measurements and the mean water level on the reef flat is slightly underestimated by the model. These results suggest only infragravity wave runup is not sufficient to reproduce the total amount of wave runup at Roi-Namur, and the incident wave runup might have a significant contribution.

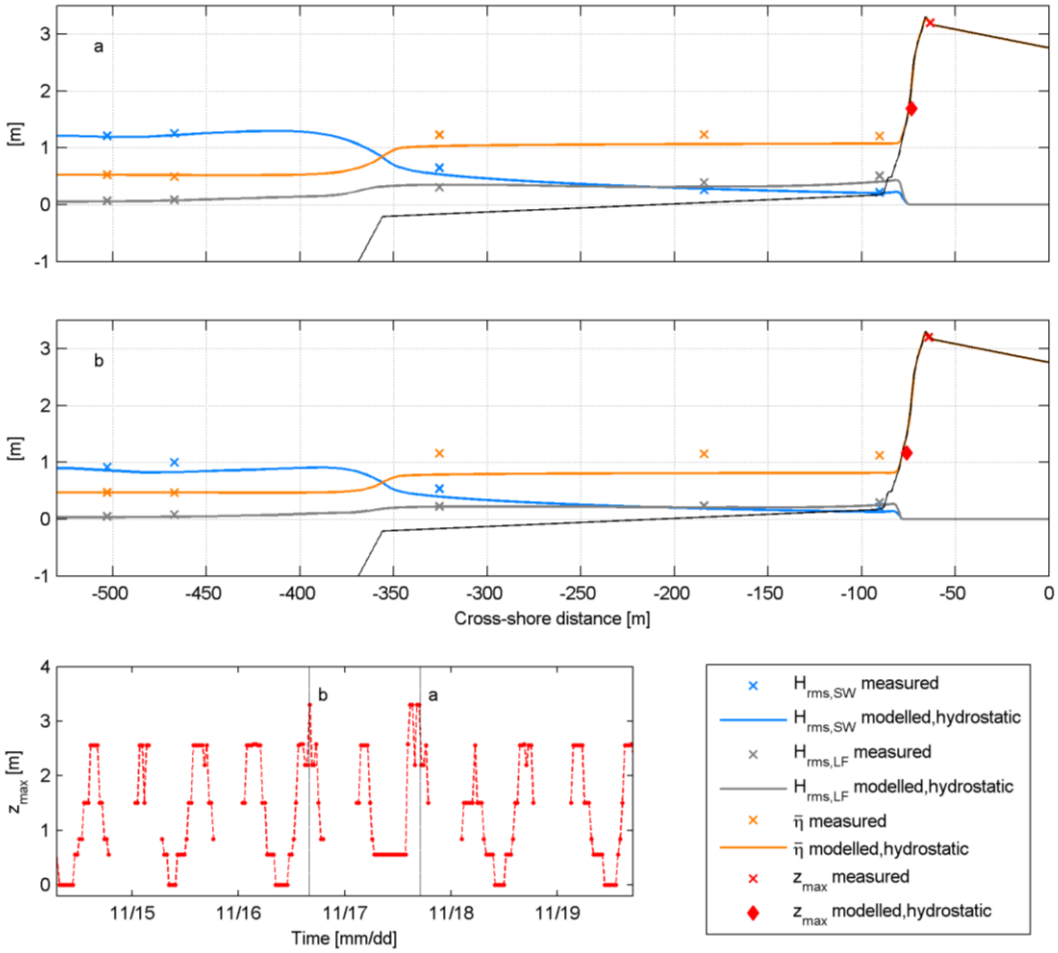

Figure 4.10 Spatial distribution of the peak wave runup simulations for events 'a' and 'b' (indicated in the bottom panel). The modelled infragravity wave runup is denoted with the red diamond, the measured z_{max} is indicated with the red 'x'.

4.5 Incident wave runup

In the previous section it is shown that the measured wave runup is significantly higher than the wave runup modelled with XBeach hydrostatic. Even though the accuracy of the measured wave runup is uncertain, the difference between measured and modelled wave runup is still such that it seems the model is missing something. As XBeach hydrostatic only resolves the infragravity wave runup, it is suggested there is a contribution by the incident wave runup. In the XBeach non-hydrostatic model both high and low frequency waves are fully resolved, hence it is expected the wave runup is higher. Therefore, in this section XBeach non-hydrostatic is used to model the (infragravity and incident) wave runup at Roi-Namur.

For the non-hydrostatic simulations the model setup of the hydrostatic simulations is applied, again with a JONSWAP spectrum imposed at the offshore model boundary. In addition, the following alterations are necessary:

- The non-hydrostatic pressure correction is turned on.
- The computational grid size is smaller, as the waves are solved individually. The minimum grid size is 0.25 m and is applied from the reef crest up to the shoreline.
- One hour simulations to limit the computation time.

First in section 4.5.1 the key hydrodynamic processes across the reef during the March event are considered by re-evaluating the friction coefficients. Subsequently the optimal settings for the non-hydrostatic model are applied to model the peak runup event in November in section 4.5.2.

4.5.1 Re-evaluation of the friction coefficients

The XBeach non-hydrostatic model fully resolves the high and low frequency motions, so no wave action balance is needed (section 3.2.2). Therefore, for the non-hydrostatic simulations the only relevant friction coefficient is c_f.

The two specific moments during the March event that were discussed in section 4.3 are simulated again and are consistent with the two moments shown in Figure 4.5. First, the same friction coefficient settings are used as for the calibrated hydrostatic model, referred to as ‘simulation N1’. Subsequently, the friction coefficients are re-evaluated for the XBeach non-hydrostatic model. The results are presented in Figure 4.11, showing the spatial distribution of the mean water levels, long and short wave height along the cross-section of the reef for the two moments. The applied friction coefficients of the plotted simulation results are summarized in Table 4.4. Again, the blue points and lines are during low tide and represent the peak wave event in March. The green points and lines represent the hydrodynamics during the high tide six hours before the peak event.

Table 4.4 Friction coefficients applied in simulation N1 and N2.

Simulation	$c_{f\ fore}$ *[-]*	$c_{f\ reef\ flat}$ *[-]*
N1	0.4	0.01
N2	0.003	0.003

In simulation N1 the same friction coefficients are applied as for simulations C1 and V1 with the hydrostatic model. In Figure 4.11 the results of simulation N1 are presented with the dotted line and show a significant underestimation of the hydrodynamics across the reef. As there is too much dissipation of wave energy along the fore reef, the modelled water levels on the reef flat are considerably underestimated. Therefore the value of friction coefficient c_f is re-evaluated to better reproduce the hydrodynamics across the reef. Both (spatially varying) friction coefficients need to be lowered significantly in order to increase the water level on the reef flat. For simulation N2 a c_f of 0.003 is applied, which is consistent with the friction coefficient applied at sandy bed, and is presented by the solid lines in Figure 4.11. The results of simulation N2 approaches the measured values, but the water level is still underestimated by approximately 0.5 m on the reef flat. However, a further decrease of the friction coefficient value does not result in an increasing water level on the reef flat.

This suggests the wave-induced setup is underestimated by the XBeach non-hydrostatic model and cannot be corrected by changing the friction coefficients. In the hydrostatic model the results obtained for the wave-induced setup are much better. It is argued that this is due to compensation by over-calibration. The relatively high value of the current friction coefficient along the fore reef (c_f = 0.4) compensates for this deficiency in setup due to wave breaking. A higher c_f value results in more energy dissipation along the fore reef, which results in a higher radiation stress gradient and therefore more wave-induced setup on the reef flat.

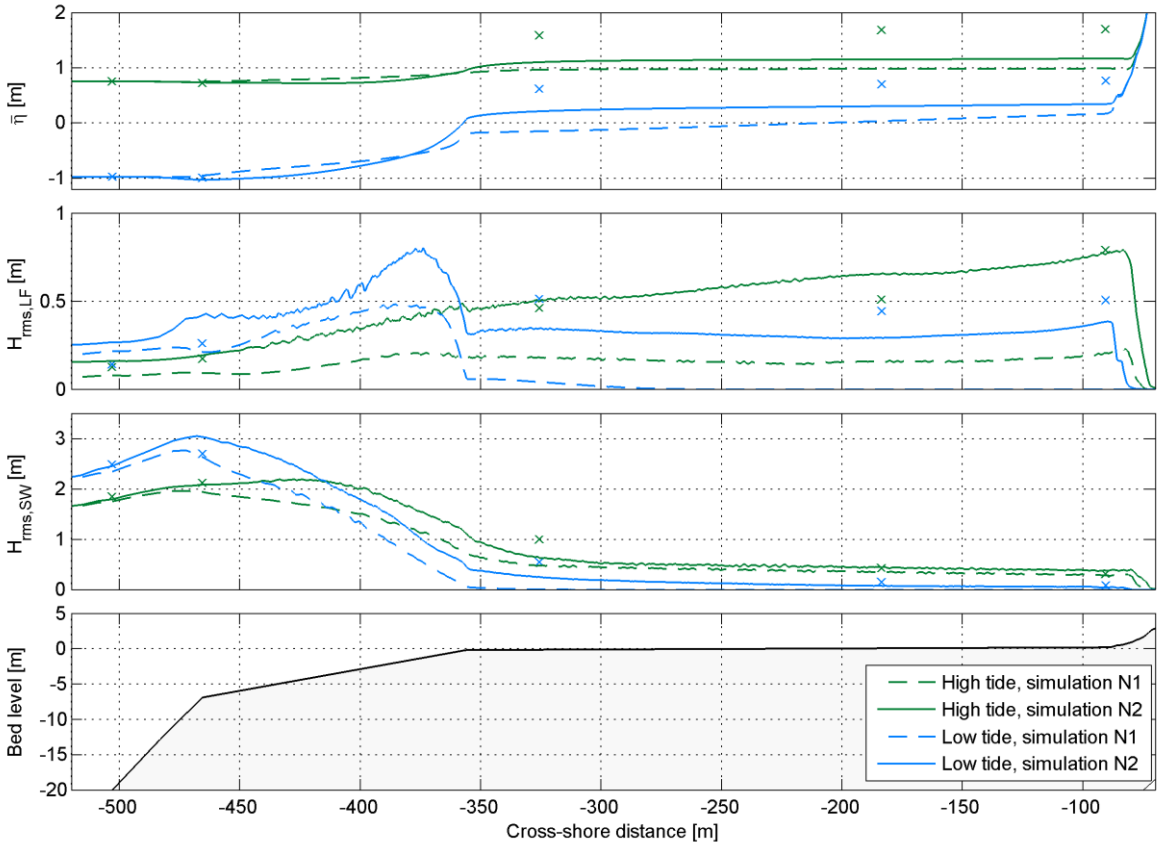

Figure 4.11 Cross-section of the XBeach non-hydrostatic results and the measured values. Blue is during the peak wave event, green 6 hours before the peak event. Friction coefficients applied in each simulation are according to Table 4.4.

The underestimation of the wave-induced setup in the non-hydrostatic model can be caused by errors in the wave breaking process. Possible reasons for this underestimation can be related to the bathymetry or the definition of wave breaking in XBeach non-hydrostatic. To further investigate this issue, additional simulations are setup.

Wave breaking occurs mainly along the steep fore reef, so the shape of the fore reef bathymetry can have an effect on the wave-induced setup. The exact bathymetry profile was not known for the most offshore located measurement location up to the outer reef flat pressure sensor, and therefore a linear interpolation was made between the known points. A more detailed bathymetry profile of the fore reef was measured during this study and is shown in the bottom panel in Figure 4.12. Simulations with this new bathymetry show a small increase in mean water level on the reef flat (top panel in Figure 4.12) of 0.10 m maximum. However, the mean water level on the reef flat is still significantly underestimated.

Secondly the definition of wave breaking in non-hydrostatic models in general may be an issue. In the non-hydrostatic model not wave heights are resolved, only the water depth. Therefore, to determine the energy dissipation of waves the non-hydrostatic model uses a wave steepness criterion (*H/L*). If this steepness is exceeded in the model, the non-hydrostatic pressure term is turned off and a breaking wave becomes analogous to a hydraulic jump. The energy dissipation can subsequently be determined by conservation of mass and momentum. However, the wave steepness criterion in the non-hydrostatic model is user defined. If this criterion is reached too early in the model, wave breaking occurs too early and the wave-induced setup is underestimated. In Figure 4.13 results of the simulations with a varying wave steepness criterion, ‘maxbrsteep’, are presented. It can be concluded the ‘maxbrsteep’-parameter has no effect on the wave-induced setup.

Additionally, there could be 2D effects present at Roi-Namur which are not accounted for in the 1D model. For example, the presence of wave-driven circulation cells on the reef flat due to differences in the two-dimensional bottom profile. This can influence the mean water levels and wave heights across the reef.

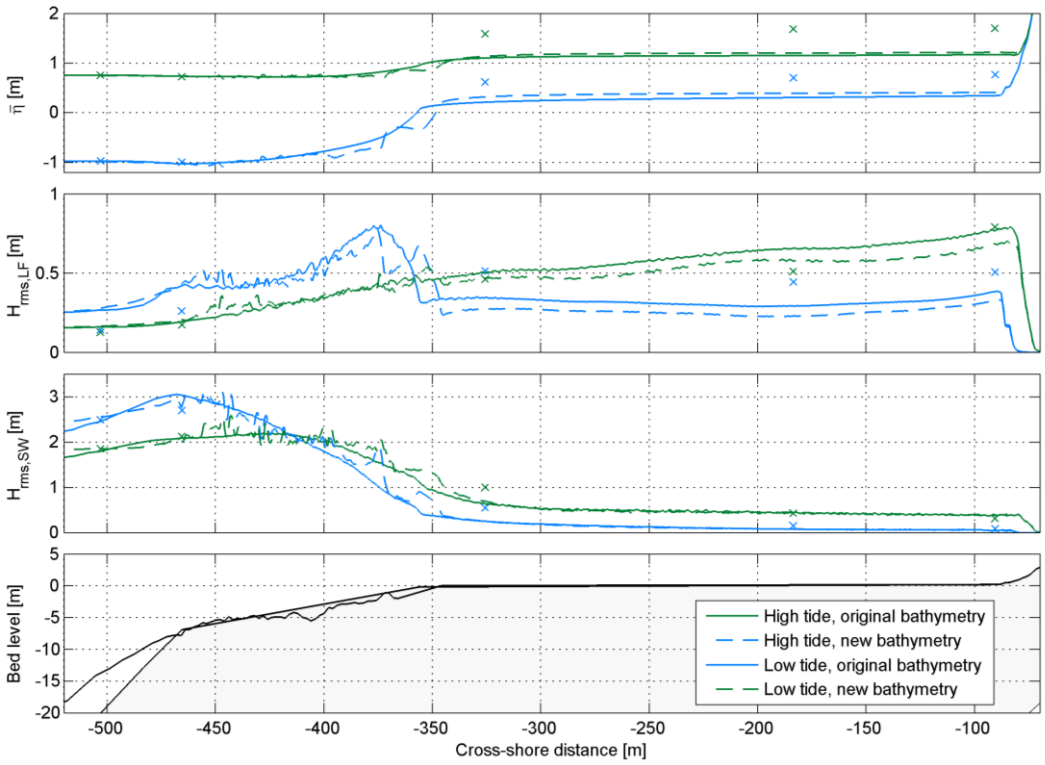

Figure 4.12 Cross-section of the XBeach non-hydrostatic results with the original bathymetry (solid line) and new bathymetry (dotted line) and the measured values. Blue is during the peak wave event, green 6 hours before the peak event.

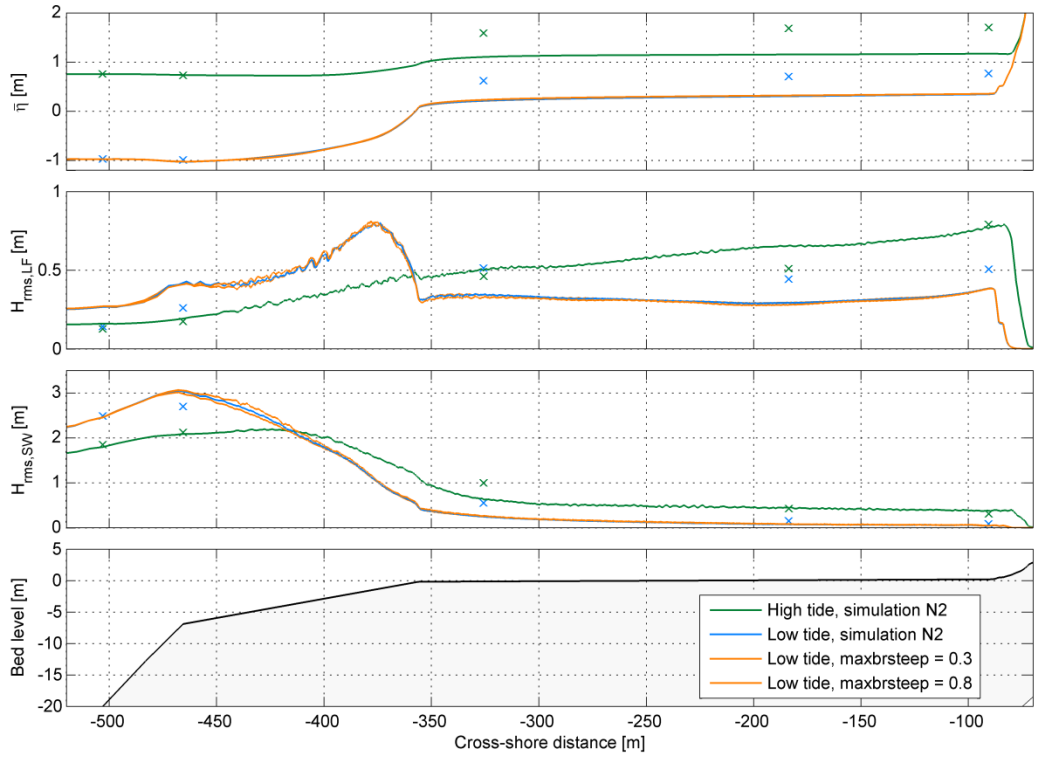

Figure 4.13 Cross-section of the XBeach non-hydrostatic results and the measured values ('x'). Blue is during the peak wave event, green 6 hours before the peak event and orange during the peak wave event with a varying wave steepness criterion ('maxbrsteep').

4.5.2 Validation

Now the XBeach non-hydrostatic model is used to reproduce the infragravity and incident wave runup at Roi-Namur. The model settings from simulation N2 (Table 4.4) are applied as the IG and short wave heights at the inner reef flat are reasonably well reproduced for the March event (Figure 4.11). The model results are validated with the peak wave runup event in November, which is analysed in section 2.4.2. Again, the two moments with the highest wave runup observed in the measurements are selected, event ‘a’ and ‘b’, as can be seen in the bottom panel in Figure 4.14.

Figure 4.14 shows the results of both simulations in the two top panels. Comparing the z_{max} results with the results from the hydrostatic model in Figure 4.10, it is shown the modelled z_{max} is higher for the non-hydrostatic simulations. Despite the underestimated modelled water levels on the reef flat, the modelled z_{max} is 0.3 m and 0.4 m higher for respectively event ‘a’ and ‘b’.

Although the water levels on the reef flat are underestimated by the model, the maximum runup is higher as with the hydrostatic simulations. This suggests there is a significant contribution of the incident wave runup to the total wave runup for these particular events. The additional effect of incident wave runup is expected to be even larger if the water levels on the reef flat are correctly modelled, as the short wave height on the reef flat strongly depends on the water depth. Thus, the non-hydrostatic model gives a better approximation of the runup at the Kwajalein Atoll, but still does not reach the measured maximum runup value at Roi-Namur. Contrary to the hydrostatic model, this seems to be related to the underestimation of the wave-induced setup at the reef flat.

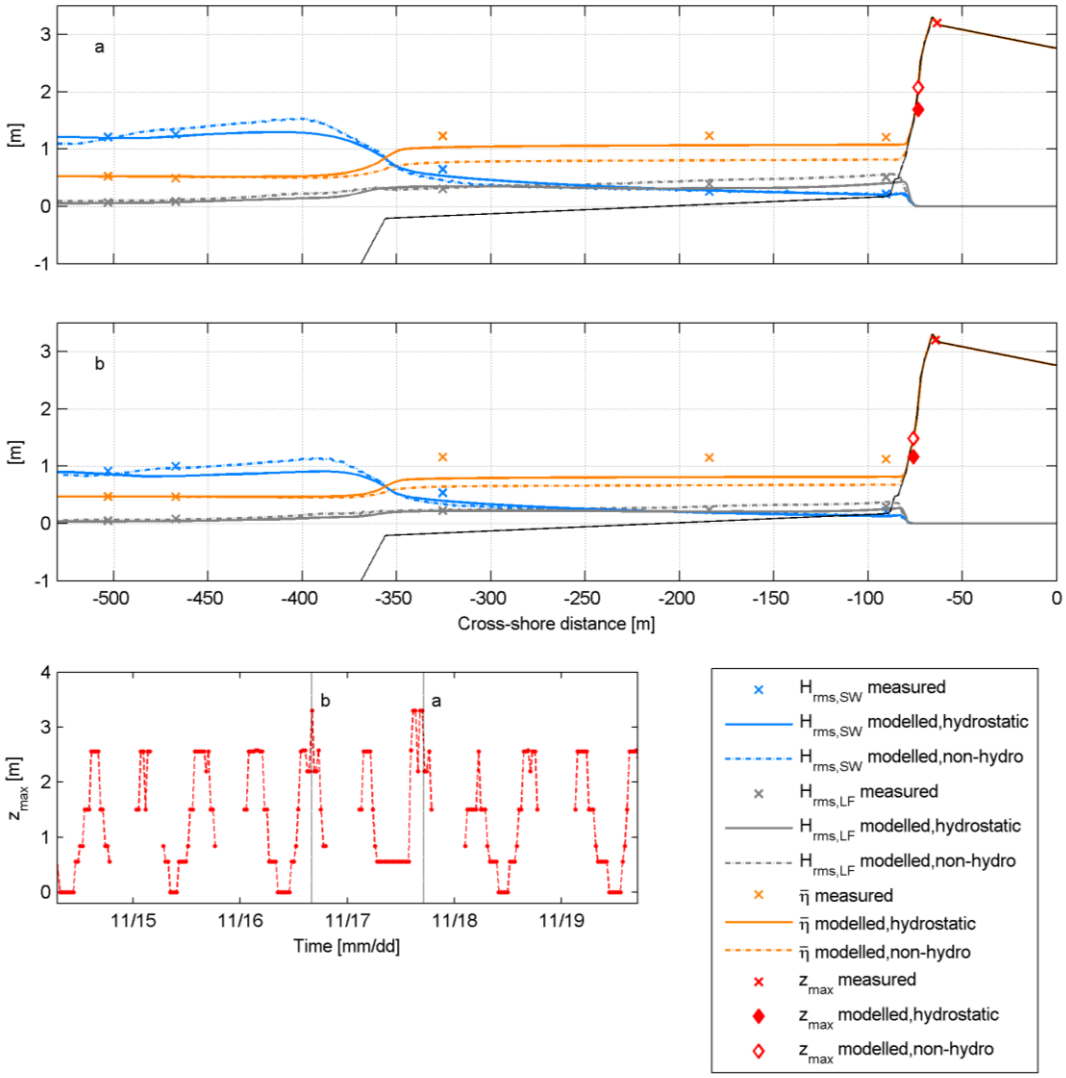

Figure 4.14 Spatial distribution of the peak wave runup simulations for events 'a' and 'b' (indicated in the bottom panel). The modelled infragravity and incident wave runup is denoted with the red diamond, the measured z_{max} is indicated with the red 'x'.

4.6 Discussion

The main conclusion which can be drawn from this chapter is that the wave runup is underestimated by both the hydrostatic and non-hydrostatic model for the Kwajalein Atoll. This is in contrast with the simulated hydrodynamics across the reef flat, which are in good agreement with the measurements. However, it can be discussed whether a mean water level of 1.2 m, an infragravity and short wave height of 0.5 m and 0.3 m respectively can result in a maximum wave runup up to 3.3 m (event 'a' in Figure 4.10 and Figure 4.14).

In order to explain this observed peak wave runup event, the measured burst of data of the inner reef flat pressure sensor belonging to the peak runup event 'a' is shown in Figure 4.15. It is noticed there is a peak in the surface elevation around 16:17, which reaches up to a water level of 2.3 m. The wave runup photo belonging to the peak wave runup event (Figure 2.11) is taken at 16:17 on 17 November 2013, which was at the exact moment of the instantaneous peak in surface elevation as shown in Figure 4.15. This suggests the peak runup event is the result of this instantaneous increase in surface elevation at the inner reef flat location.

However, in this study the Kwajalein Atoll data (chapter 2) and the model results (chapter 4) are analysed by translating the obtained raw data bursts into hourly burst-averaged water levels and wave heights. These burst-averaged hydrodynamic parameters are used to force the model and subsequently validate the model. Therefore, this instantaneous peak in surface elevation is not reproduced by the simulations.

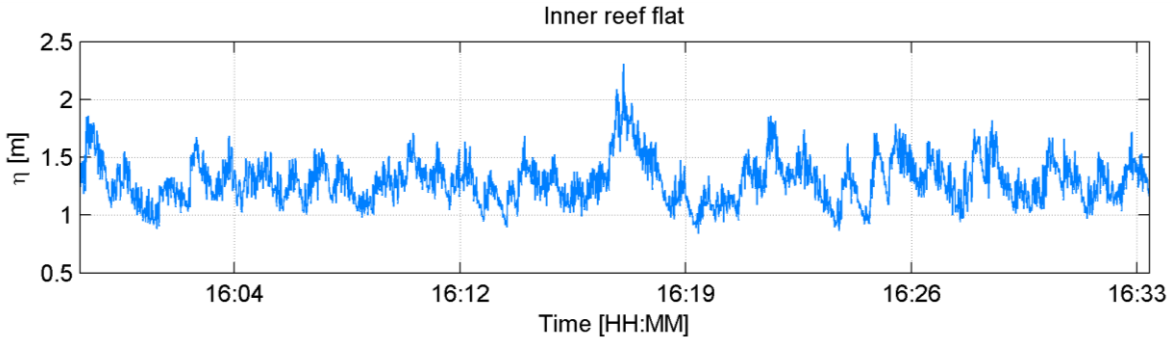

Figure 4.15 Burst surface elevation of the inner reef flat pressure sensor on 17 November 2013.

The instantaneous increase in surface elevation can be modelled by XBeach non-hydrostatic model. This can be accomplished by imposing the surface elevation time series of the burst at the offshore boundary of the model. In Figure 4.16 the results of this simulation are shown. As the non-hydrostatic model does not correctly reproduces the wave-induced setup at Kwajalein Atoll (section 4.5.1), the water levels on the reef flat are generally underestimated by the model. But the instantaneous increase in water level at the inner reef flat is indeed simulated and the modelled z_{max} for this simulation is 2.7 m.

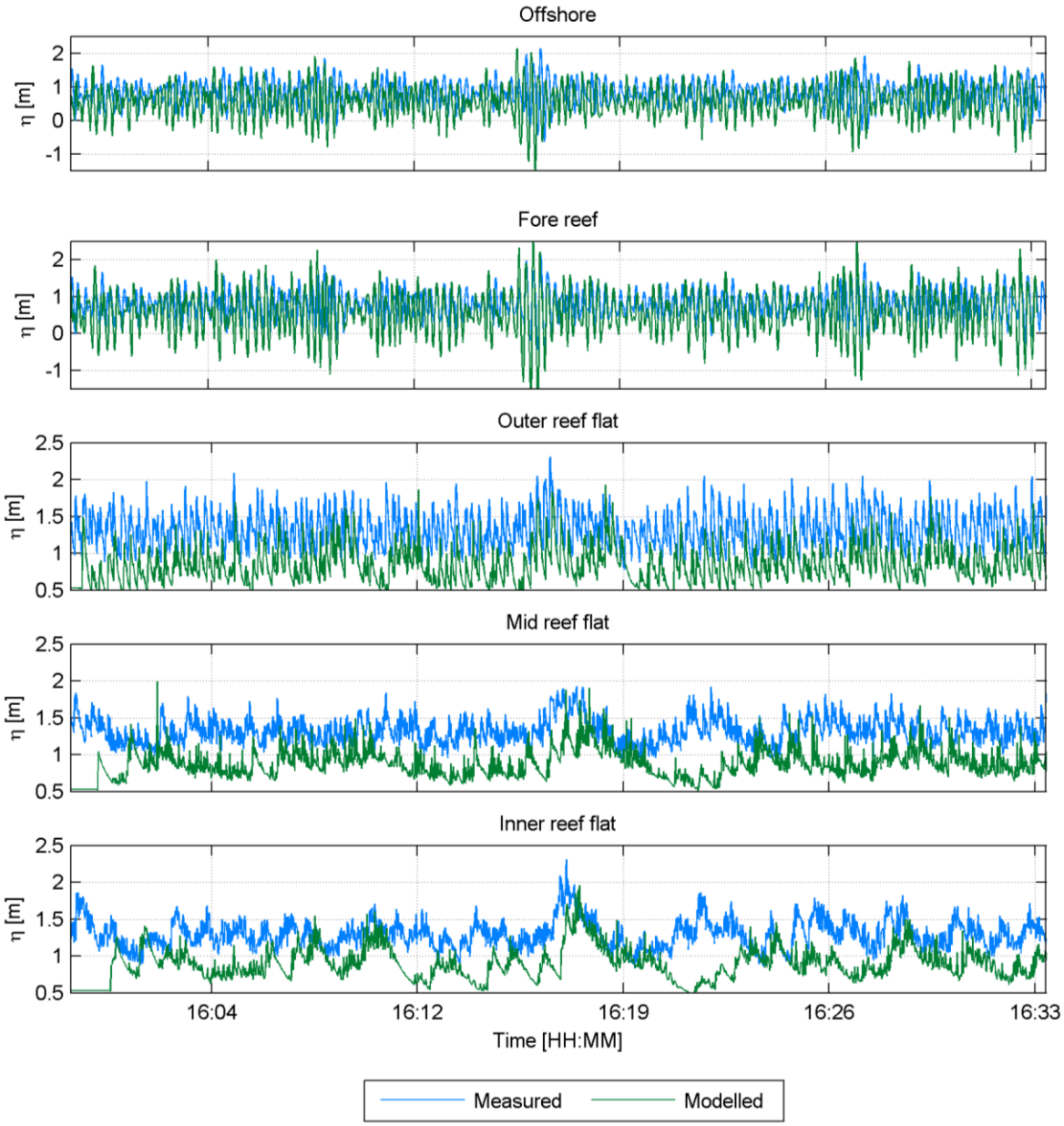

Figure 4.16 Modelled versus measured surface elevation time series for the peak wave runup event on 17 November 2013.

4.7 Conclusions

The applicability of the XBeach model to reproduce the wave runup at Kwajalein Atoll was tested using the Kwajalein Atoll data. The two energetic wave events, i.e. March and December event, were used for respectively calibration and validation of the hydrodynamics across the reef. The extreme runup event in November was used for validation of the wave runup.

The hydrodynamics across the reef were simulated accurately with the hydrostatic model of XBeach. The XBeach hydrostatic model proved to predict the hydrodynamics across the reef accurately for the following (spatially varying) friction coefficients: f_w = 0.15, $c_{f,fore\ reef}$ = 0.4 and $c_{f,reef\ flat}$ = 0.01. The model was tested for a variety of offshore wave conditions and the results were in very good agreement with the measurements. Although the model performs very well for the hydrodynamics across the reef, the extreme wave runup event was significantly underestimated by the hydrostatic model.

The non-hydrostatic model of XBeach provides a better approximation of the wave runup, as it calculates both the IG and the incident wave runup components. However, the mean water level on the reef flat was underestimated. This was attributed to incorrectly modelling of the wave-induced setup on the reef flat. It was demonstrated that a more detailed bathymetry profile of the fore reef or adjusting the maximum wave steepness criterion in XBeach did not resulted in a better approximation of the wave-induced set-up.

Further analysis of the extreme runup event showed this event was caused by a moment with a significantly higher instantaneous water level, which was not accounted for by the burst-averaged mean water level. Therefore, a new non-hydrostatic XBeach simulation was setup in which the measured instantaneous water level time series was applied at the offshore boundary. This resulted in a significant increase in the instantaneous water level and subsequently wave runup. There was, however, still an underestimation of the measured wave runup found. This was attributed to the (still) incorrectly modelled wave-induced set-up.

It can be concluded that for the measured extreme wave runup event at Kwajalein Atoll, it is not sufficient to schematize the hydraulic conditions into hourly burst-averaged characteristics. However, it is important to keep in mind this analysis is based on only one observed extreme runup event, which was the result of an instantaneous increase in the surface elevation.

5 Conceptual model for wave runup on atoll reefs

5.1 Introduction

The inundation events are not only causing problems at the Kwajalein Atoll, but are affecting atoll islands throughout the Pacific and Indian Oceans. These atoll reefs have strongly varying reef dimensions, topography and wave and tidal conditions. The site specific characteristics can have an impact on the forces driving the inundation events, and therefore the wave runup at the beach.

The knowledge gathered in the previous chapters on the Kwajalein Atoll hydrodynamics can be used to provide a first indication of the impact of site specific characteristics on wave runup at atoll reefs. Although the XBeach gives an accurate prediction of the hydrodynamics across the Kwajalein reef, the model underestimates the extreme runup events at Kwajalein. However, the XBeach model can be used to test the relative impact on runup for changing reef dimensions, topography and wave and tidal conditions. In this chapter an idealized one-dimensional cross-shore profile of an atoll reef is defined to create a conceptual model with XBeach. The main purpose of this conceptual model is to test the sensitivity of wave runup to variations in the atoll reef parameter space.

First in section 5.2 the parameter space of atoll reefs in general are determined. Section 5.3 presents the methodology for the sensitivity analysis with the conceptual model. Subsequently the results of the conceptual model are presented in section 5.4. Finally, the conclusions regarding the conceptual model results are discussed in section 5.5.

5.2 Atoll reef parameter space

The ocean side of a typical atoll reef is generally characterized by a steep fore reef slope, a relatively long reef flat and rough bottom topography. Due to their variation in location, history and hydrodynamics conditions, the values of these characteristics can vary significantly. To identify typical values of atoll reef characteristics, i.e. the parameter space, a literature review is conducted. The resulting atoll reef parameter space is presented in Table 5.1. The defined parameter space consists of reef dimension parameters, i.e. reef flat width, fore reef slope and beach slope, and a hydrodynamic parameter, i.e. water depth on the reef flat. Bottom roughness is also an important parameter and varies significantly per atoll reef, but is not included in the review. Bottom roughness is a difficult parameter to quantify, and is not defined in many studies. However, it will be included in the conceptual model.

It is noted a number of fringing reefs are also included in the review as their characteristics correspond strongly with a typical atoll reef. The fringing reefs included in the review have a relatively small and shallow lagoon and are therefore very similar to atoll reefs.

Table 5.1 Atoll reef parameter space cited in literature.

		Reef dimensions			**Hydrodynamic**
Reef type	*Location*	*Fore reef slope [-]*	*Reef flat width [m]*	*Beach slope [-]*	*Reef water depth [m]*
Fringing	Ningaloo reef, Australia[1]	1/20	1000	-	1,00 – 2,00
Fringing	Lady Elliot Island, Australia[2]	-	50 - 400	1/7 - 1/12	0,80 – 1,70
Atoll	Mururoa, French Polynesia[3]	-	100	-	0,60
Fringing	Ipan, Guam[4]	1/16	400	-	0,10 – 1,10
Fringing	Hanalei reef, Hawaii[5]	1/18	300	-	1,00 – 1,40
Fringing	Molokai, Hawaii[6]	1/18	500 - 1000	vertical	0,30 – 2,00
Fringing	Male, Maledives[7]	1/1	140	-	1,30 – 3,80
Atoll	Majuro, RMI[8]	1/7	250	-	0,80 – 1,00
Atoll	Kwajalein, RMI	1/20	250	1/6	0,00 – 1,00
Atoll	Alphonse, Seychelles[9]	1/10 - 1/20	400 - 500	1/10	0,00 – 0,20
	maximum value	1/1	1000	vertical	3,80
	minimum value	1/20	50	1/12	0,00

[1] Pomeroy et al. (2012); van Dongeren et al. (2013*)*

[2] Jago et al. (2007); Huang et al. (2012*)*

[3] Tartinville and Rancher (2000*)*

[4] Péquignet et al. (2009); Vetter et al. (2010); Becker et al. (2014*);* Péquignet et al. (2011*)*

[5] Hoeke et al. (2013*)*

[6] Presto et al. (2006*);* Storlazzi et al. (2004*);* Storlazzi et al. (2011*)*

[7] Jensen (1991*)*

[8] Becker et al. (2014*)*

[9] Hagan and Spencer (2008); Hamylton (2011*)*

5.3 Methodology

The sensitivity of wave runup and its components, i.e. setup, IG and incident swash, to variations in the atoll reef parameter space is tested with a conceptual model. This section presents the setup of the conceptual model and subsequently the methodology for post-processing the wave runup output into wave runup statistics.

5.3.1 Conceptual model setup

To test the sensitivity of wave runup to variations in the parameter space, a conceptual model is constructed with an idealized 1D cross-shore atoll reef profile. The idealized 1D cross-shore profile is constructed based on the literature review and the Roi-Namur bathymetry profile, and is shown in Figure 5.1. The dimensions and hydrodynamic conditions of Roi-Namur will serve as a reference case for the conceptual model simulations. The simulations are conducted for a period of one hour. At the offshore boundary a Jonswap spectrum is imposed which is generated from the peak wave event in March. During this event the offshore significant wave height was 3.51 m and the peak wave period 15 s. For each simulation a parameter of the reference case is varied, while the other parameters are kept constant at the reference case value.

The range in parameter values for the conceptual model simulations are defined based on the literature review presented in section 5.2. The reef flat water depth parameter is translated into a parameter representing the variation in the offshore tidal elevation. The water depth on the reef flat strongly depends on the wave-induced setup and can therefore not be imposed in the model. In addition, the friction coefficients are added to the conceptual model parameter space. As for the Roi-Namur reef, a spatially varying friction coefficient is taken into account. The parameters and their range for simulations in the conceptual model are summarised in Table 5.2.

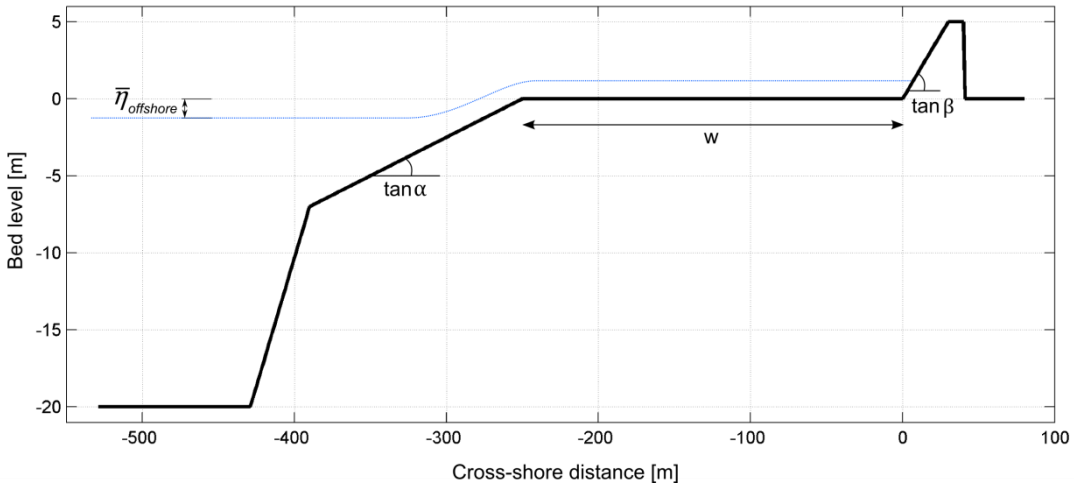

Figure 5.1 Conceptual model setup with the idealized 1D cross-shore profile of the reference case and the relevant parameters indicated.

Table 5.2 Parameter space for the conceptual model.

Symbol	*Parameter*		*Reference case*	*Range for simulations*
tanα	Fore reef slope	[-]	1/12	1/100 – 1/1
w	Reef flat width	[m]	250	50 – 1000
tanβ	Beach slope	[-]	1/6	1/12 – 2/1
$\overline{\eta}_{offshore}$	Offshore tidal elevation	[m]	- 0.9	-1.50 – 2.00
$c_{f,reefflat}$	Current friction reef flat	[-]	0.01	0 – 0.5
$c_{f,fore\ reef}$	Current friction fore reef	[-]	0.4	0 – 0.5
f_w	Wave friction	[-]	0.15	0.03 – 0.6

5.3.2 Calculation of wave runup statistics

Wave runup is commonly represented by the 2% exceedence value, $R_{2\%}$, and consists of setup and swash. In addition, swash can be separated into incident and IG swash. These four measures of wave runup are calculated from the runup output of each simulation using the method of Stockdon et al. (2006) , which is visualized in Figure 5.2.

The extracted runup from the runup gauge in XBeach is a continuous water level time series of the detected shoreward-most wet point. The time-averaged water level of this runup time series is defined as the setup at the shoreline. The incident and IG swash is calculated from the spectra of the runup time series, by using a similar method as for the separation of waves (section 2.3.1). The swash components are separated with the split frequency (f_{split} = 0.04 Hz) and subsequently the significant swash is calculated according to equation [2.5]. The 2% exceedence value of runup is calculated from the cumulative probability density function of the individual runup maxima in the runup time series.

The runup heights are associated with the individual runup peaks in the water level time series, as depicted in the top panel in Figure 5.2, and includes the wave setup and swash. In this study the individual runup maxima (R) are determined on an infragravity wave period time scale, as only the extreme runup maxima are of interest. The time filter is based on the split frequency separating the short wave and infragravity frequency bands. The split frequency is defined as half of the offshore peak frequency (Roelvink & Stive, 1989), which resulted in a filter time scale for maximum runup heights of four times the incident wave period.

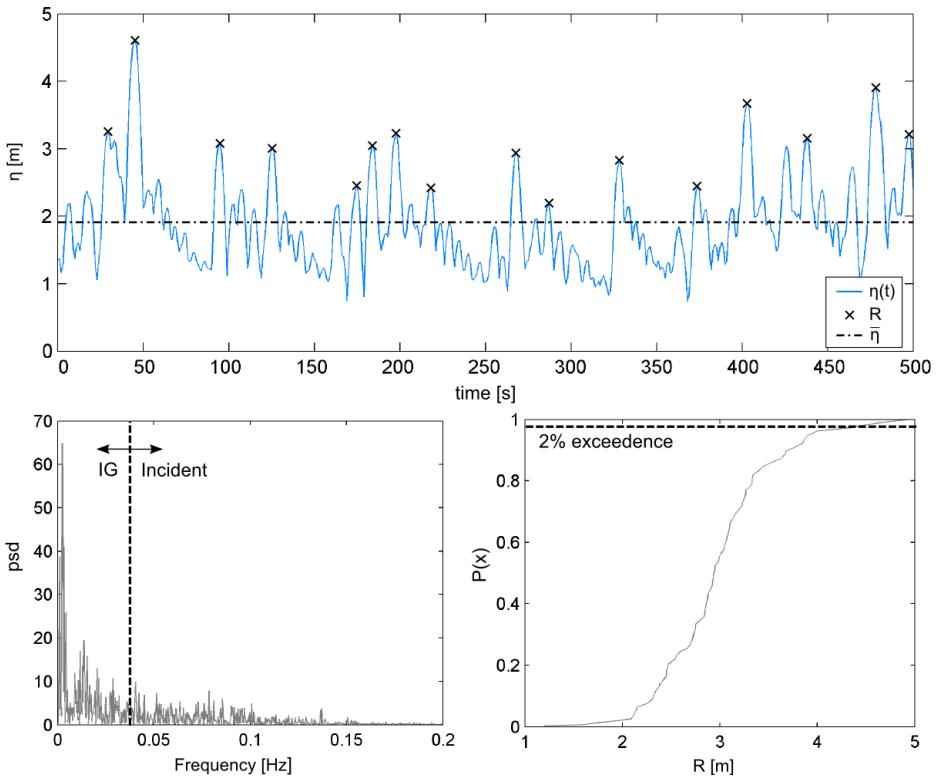

Figure 5.2 Runup time series (partly) extracted from a XBeach simulation (top panel), indicating the mean water level at the shoreline ($\bar{\eta}$) and the individual runup maxima (R). The spectrum generated from the runup time series for calculating the swash statistics (bottom left panel). The cumulative probability function of the R measures (bottom right panel) for calculating the 2% exceedence value of runup. Figure is based on Stockdon et al. (2006).

5.4 Conceptual model results

The sensitivity of wave runup and its components, i.e. setup, IG and incident swash, to variations in the parameter space is tested with a conceptual model. In this section the results of the conceptual model simulations are presented, using the methodology described in the previous section.

First the results of the conceptual model simulations with the XBeach hydrostatic model are shown in section 5.4.1. Subsequently in section 5.4.2, the results of the same simulations are presented, but now the XBeach non-hydrostatic model is used. Despite its limitations in reproducing the setup on the Roi-Namur reef flat (section 4.5.1), the non-hydrostatic model can test the response of incident wave runup to variations in the parameter space.

5.4.1 Infragravity wave runup

In Figure 5.4 the results of the conceptual model simulations are shown. The response of the wave runup ($z_{2\%}$) and its components, i.e. incident swash (S_{inc}), IG swash (S_{IG}) and mean water level at the beach ($\bar{\eta}$) are plotted against the variations in the parameter space. In order to consistently compare the results with the same reference level, the mean water level ($\bar{\eta}$) is plotted instead of the total wave-induced setup. In addition, the $z_{2\%}$ is shown instead of the $R_{2\%}$. All results are hereby shown with respect to the reef flat reference level as in Figure 1.1.

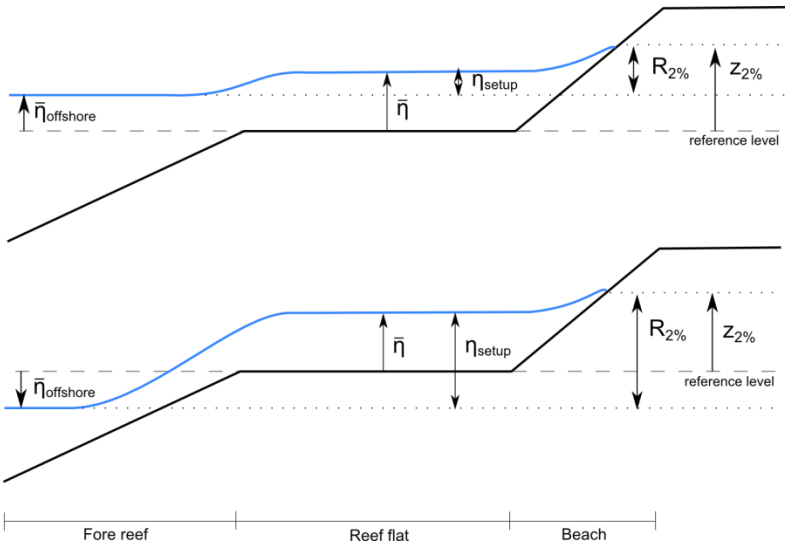

Figure 5.3 Idealized 1D cross-shore profile of an atoll reef including key features and the definition of wave runup and its components

In general the incident swash has a very low value and shows little variability, as is expected for simulations with the XBeach hydrostatic model.

A variation in reef flat width does not result in a significant change in wave runup. As nothing changes in the offshore wave conditions and the shape of the fore reef, the amount of wave-induced setup generated on the fore reef does not change. Therefore the mean water level on the reef flat is constant for a varying reef flat width. However, if the reef flat width becomes smaller than 200 m, the S_{IG} and $z_{2\%}$ slightly increases. This suggests there is some wave energy dissipation along the reef flat due to bottom friction, which is not dissipated if the reef flat width is relatively small.

The variation in fore reef slope demonstrates the $z_{2\%}$, S_{IG} and S_{inc} all become larger as the fore reef slope steepens. This can be explained with the horizontal momentum balance in equation [2.6]. As the fore reef becomes steeper, wave energy dissipation due to wave breaking occurs along a smaller distance. The radiation stress gradient therefore increases and subsequently the setup becomes larger. As the water depth on the reef flat is now larger, the wave heights across the reef flat are higher which results in a higher wave runup. It is noted that if the fore reef slope is steeper than 1/6, the simulations fail due to (too) high velocities at the reef crest.

IG wave runup and its components are not responding to changes in the beach slope. This corresponds with the formulations of Stockdon et al. (2006) where the S_{IG} only depends on the offshore wave height and length.

The most notable change in wave runup is demonstrated as the offshore mean water level is adjusted. Although the wave-induced setup decreases as the offshore water level increases, the $z_{2\%}$ continues to increase. Due to the higher water levels on the reef flat, more and higher waves are present across the reef and therefore the IG swash increases at the beach. This tidal dependency is consistent with the results from the data analysis in section 2.3.4.

Overall, the friction coefficients in the model have an effect on the wave runup. Increasing the fore reef current friction ($c_{f,fore\ reef}$) generates more wave-induced setup on the reef flat (as discussed in section 4.5.2) and therefore higher wave runup is modelled. The current friction coefficient on the reef flat only affects the IG waves, which is also demonstrated by the modelled IG swash. For $c_{f,reef\ flat}$ values higher than 0.2 the simulations fail due to high velocities. A higher f_w value results in higher wave energy dissipation in the wave action balance of the hydrostatic model. Consequently, less wave energy is present towards the shore and less wave runup is simulated. It can be concluded generally a higher bottom roughness results in a decreasing wave runup. This is in contrast with the fore reef current friction coefficient, where a higher friction results in more wave runup. It is argued this is the result of compensation of the wave-induced setup by over-calibration, as discussed in section 4.5.1.

Summarizing, the most significant variations in wave runup is expected for parameters influencing the mean water levels on the reef flat. The main parameters causing this changing water depth on the reef flat are the offshore water level, the fore reef slope and the friction coefficients. The last two parameters have an effect on the wave energy dissipation along the fore reef, which affects the wave-induced setup on the reef flat. Furthermore, a higher wave runup can be expected for a relatively low reef flat width.

However, the effect of incident swash on the total wave runup is not included in this sensitivity analysis. The incident swash is generated by the short wave motions near the beach. In chapter 2 it was concluded the short wave heights across the Kwajalein reef flat strongly depends on the water depth on the reef flat. Since Figure 5.4 suggests that variations in the parameter space can result in higher mean water levels on the reef flat, an increase of the incident swash is expected as a consequence of the increasing water depth. Therefore, it is expected the incident swash can contribute significantly to the total wave runup for certain variations in parameter space. In the next section the XBeach non-hydrostatic model is used to include the incident swash in the sensitivity analysis.

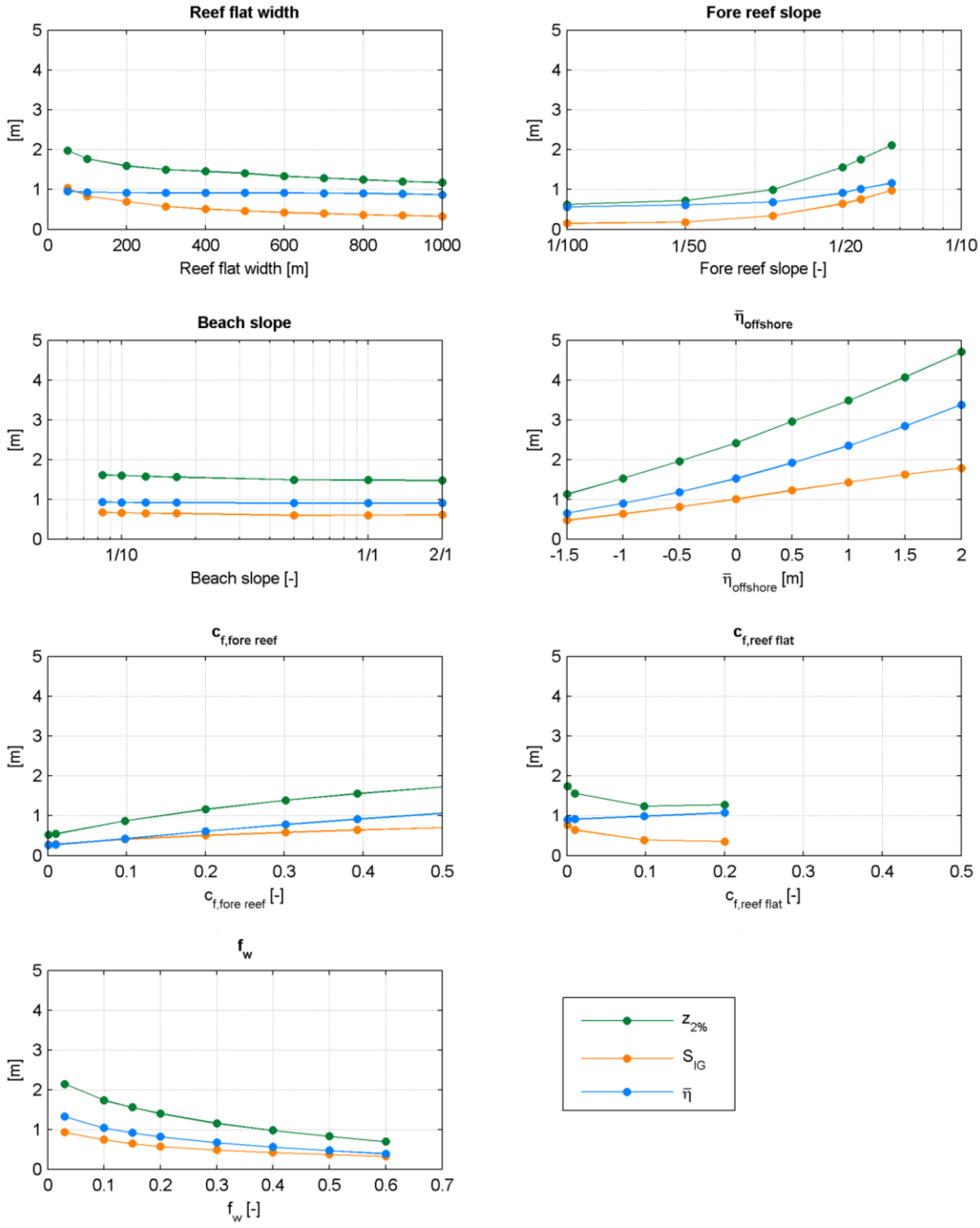

Figure 5.4 Conceptual model results for the infragravity wave runup. Response of $z_{2\%}$, incident swash (S_{inc}), IG swash (S_{IG}) and mean water level ($\bar{\eta}$) to variations in reef dimensions (i.e. reef flat width, fore reef slope, beach slope), friction coefficients (i.e. f_w, $c_{f,fore\ reef}$, $c_{f,reef\ flat}$) and offshore water level ($\bar{\eta}_{offshore}$).

5.4.2 Incident wave runup

In this section the effect of the incident swash is included in the sensitivity analysis by using the XBeach non-hydrostatic model. Despite its limitations in accurately modelling the wave-induced setup (section 4.5.1), it can give an indication of the impact of incident swash on the total wave runup. Again, the conceptual model setup, presented in section 5.3, is used to test the sensitivity of wave runup to variations in the parameter space. As the non-hydrostatic model is used to capture the incident swash motions, this resulted in a few alterations in the conceptual model consistent with the settings of the non-hydrostatic model in section 4.5.1;

- The non-hydrostatic pressure correction is turned on.
- The numerical grid size is reduced and varies from 0.25 m onshore to 5 m offshore.
- The applicable friction coefficients are $c_{f,fore\ reef}$ and $c_{f,reef\ flat}$, and both have a value of 0.003 in the reference case.

In Figure 5.5 the results of the conceptual model are presented for the wave runup ($z_{2\%}$) and its components, i.e. incident swash (S_{inc}), IG swash (S_{IG}) and mean water level at the beach ($\bar{\eta}$). Overall, the results of the non-hydrostatic simulations show similar patterns in the wave runup sensitivity as for the hydrostatic simulations (Figure 5.4).

Again, variations in the reef flat width no not have an effect on the mean water level at the beach. But the impact of the incident swash is significant for the smaller reef flat width values. The wave runup is higher for small reef flat widths, as less wave energy is dissipated along the (shallow) reef flat due to bottom friction.

The variations in fore reef slope and beach slope show similar $z_{2\%}$ values and patterns as were obtained with the hydrostatic simulations. However, the wave-induced setup is still underestimated by the non-hydrostatic model and can have a substantial effect on the incident swash magnitude.

The highest variability in $z_{2\%}$ is again observed for the offshore water level parameter. With the incident swash included in the model, the wave runup is significantly higher. Furthermore, a strong correlation of the incident swash with the mean water level is visible.

The friction coefficient variation simulations are consistent with the results presented in section 4.5.1. The friction coefficients need to be lowered significantly to generate enough water depth on the reef flat. It was argued the wave breaking process on the fore reef is not modelled accurately by the non-hydrostatic model, and subsequently the wave-induced setup is underestimated. Therefore, no conclusions on the influence of the friction coefficients on the wave runup are made based on Figure 5.5.

Summarising, the sensitivity of the wave runup for variations in the parameter space have similar patterns for both the hydrostatic and non-hydrostatic models. However, a significant contribution of the incident swash to the total wave runup is observed by the non-hydrostatic model despite the underestimated water levels on the reef flat. It is therefore expected the wave runup will be even higher if the water levels on the reef flat are modelled more accurately.

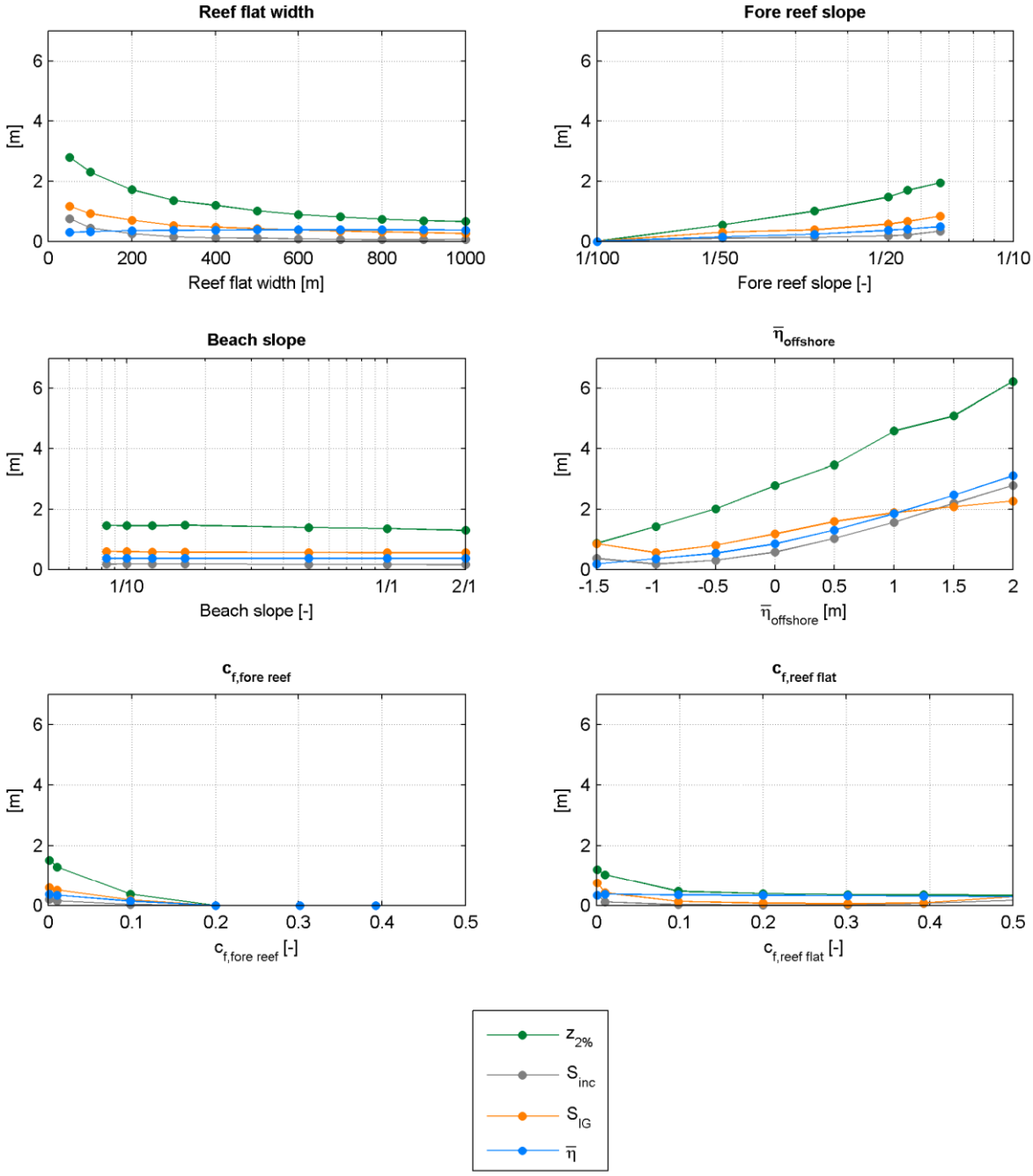

Figure 5.5 Conceptual model results for the incident wave runup. Response of $z_{2\%}$, incident swash (S_{inc}), IG swash (S_{IG}) and mean water level ($\overline{\eta}$) to variations in reef dimensions (i.e. reef flat width, fore reef slope, beach slope), friction coefficients (i.e. $c_{f,fore\ reef}$ and $c_{f,reef\ flat}$) and offshore water level ($\overline{\eta}_{offshore}$).

5.5 Conclusions

The main purpose of the conceptual model was to identify the parameters which can have a significant effect on the wave runup on an atoll reef. The response of the wave runup ($z_{2\%}$) and its components, i.e. incident swash (S_{inc}), infragravity swash (S_{IG}) and mean water level at the beach ($\overline{\eta}$) to variations in the parameter space was tested with a conceptual hydrostatic and non-hydrostatic XBeach model.

The most significant variations in wave runup were observed for parameters influencing the mean water levels on the reef flat. The main parameters causing this changing water depth on the reef flat were; the offshore water level, the fore reef slope and the friction coefficients. The last two parameters have an effect on the wave energy dissipation along the fore reef, which affects the wave-induced setup on the reef flat. Furthermore, a higher wave runup can be expected for a relatively low reef flat width.

Additionally, a significant contribution of the incident swash to the total wave runup was observed by the non-hydrostatic model despite the underestimated water levels on the reef flat. It is therefore expected the wave runup will be even higher if the water levels on the reef flat are modelled more accurately, as the short wave heights across the Kwajalein reef flat strongly depends on the water depth on the reef flat.

Combining these results and the expected rising of sea levels, it is expected the wave runup will increase in the future. Rising offshore water levels will result in less wave-induced setup on the reef flat, but will cause an increase in the amplitude of infragravity and incident swash magnitudes.

6 Conclusions and recommendations

6.1 Conclusions

The primary objective of this research was to investigate wave-induced runup on atoll reefs. This was accomplished by analysing the data obtained at Kwajalein Atoll and subsequently using this data to calibrate and validate two versions of the XBeach model for water levels, waves and wave runup. Finally, a conceptual model was created to investigate the effect of variations in the atoll reef parameter space on the wave runup. The conclusions following from this research are presented in this chapter.

Kwajalein Atoll data analysis

Field data collected from 3 November 2013 to 13 April 2014 at the Roi-Namur Island on Kwajalein Atoll was analysed to provide insight into the relevant hydrodynamic processes. During the deployment period two energetic wave events occurred, referred to as the December and March event. The March event was the most energetic event, therefore this subset of the data was used for analysis.

The wave height evolution over the reef profile shows a general trend of increasing low frequency (IG and VLF) waves and decreasing high frequency (short) waves. From the analysis it was concluded that short wave energy dissipation was the result of both wave breaking and bottom friction, as observed in previous studies. IG and VLF waves were present on the reef flat and their magnitudes increased towards the shore. This suggests frictional dissipation plays a minor role in the IG and VLF wave height evolution across the reef due to the relatively smooth reef flat. Especially during the energetic March event the IG and VLF wave heights increase substantially and become dominant at the inner reef flat. Additionally, the observations show that the short, IG and VLF wave heights on the reef flat were strongly determined by the local water depth, which is mainly the result of the offshore tidal variations. Comparing these results with the results at Ningaloo Reef by Pomeroy et al. (2012), it is suggested that the effect of frictional dissipation on the tidal modulation in IG wave heights is significant on the reef flat

The wave-induced setup on the reef flat increases as the offshore wave height increases and is reasonably constant across the reef flat. Furthermore, wave-induced setup is inversely correlated with the offshore tidal elevation due to depth-induced wave breaking on the fore reef slope. The water depth on the reef flat is therefore strongly affected by the tidal variations and the offshore wave height, and consequently affects the (short, IG and VLF) wave height on the reef flat.

Runup observations were collected for the period between 3 November 2013 and 17 December 2013 and included one extreme runup event. This is the result of a high mean water level on the reef flat and high wave heights at the inner reef flat. As the water depth increases on the reef flat, the wave heights at the shoreline increase. This results in higher maximum vertical water level excursion, z_{max}, observations.

XBeach model results

The applicability of the XBeach model to reproduce the wave runup at Kwajalein Atoll was tested using the Kwajalein Atoll data. The two energetic wave events, i.e. March and December event, were used for respectively calibration and validation of the hydrodynamics across the reef. The extreme runup event in November was used for validation of the wave runup.

The hydrodynamics across the reef were simulated accurately with the hydrostatic model of XBeach. The XBeach hydrostatic model proved to predict the hydrodynamics across the reef accurately for the following (spatially varying) friction coefficients: f_w = 0.15, $c_{f,fore\ reef}$ = 0.4 and $c_{f,reef\ flat}$ = 0.01. The model was tested for a variety of offshore wave conditions and the results were in very good agreement with the measurements. Although the model performs very well for the hydrodynamics across the reef, the extreme wave runup event was significantly underestimated by the hydrostatic model.

The non-hydrostatic model of XBeach provides a better approximation of the wave runup, as it calculates both the IG and the incident wave runup components. However, the mean water level on the reef flat was underestimated. This was attributed to incorrectly modelling of the wave-induced setup on the reef flat. It was demonstrated that a more detailed bathymetry profile of the fore reef or adjusting the maximum wave steepness criterion in XBeach did not resulted in a better approximation of the wave-induced set-up.

Further analysis of the extreme runup event showed this event was caused by a moment with a significantly higher instantaneous water level, which was not accounted for by the burst-averaged mean water level. Therefore, a new non-hydrostatic XBeach simulation was setup in which the measured instantaneous water level time series was applied at the offshore boundary. This resulted in a significant increase in the instantaneous water level and subsequently wave runup. There was, however, still an underestimation of the measured wave runup found. This was attributed to the (still) incorrectly modelled wave-induced set-up.

It can be concluded that for the measured extreme wave runup event at Kwajalein Atoll, it is not sufficient to schematize the hydraulic conditions into hourly burst-averaged characteristics. However, it is important to keep in mind this analysis is based on only one observed extreme runup event, which was the result of an instantaneous increase in the surface elevation.

Conceptual model results

The main purpose of the conceptual model was to identify the parameters which can have a significant effect on the wave runup on an atoll reef. The response of the wave runup ($z_{2\%}$) and its components, i.e. incident swash (S_{inc}), infragravity swash (S_{IG}) and mean water level at the beach ($\overline{\eta}$) to variations in the parameter space was tested with a conceptual hydrostatic and non-hydrostatic XBeach model.

The most significant variations in wave runup were observed for parameters influencing the mean water levels on the reef flat. The main parameters causing this changing water depth on the reef flat were; the offshore water level, the fore reef slope and the friction coefficients. The last two parameters have an effect on the wave energy dissipation along the fore reef, which affects the wave-induced setup on the reef flat. Furthermore, a higher wave runup can be expected for a relatively low reef flat width.

Additionally, a significant contribution of the incident swash to the total wave runup was observed by the non-hydrostatic model despite the underestimated water levels on the reef flat. It is therefore expected the wave runup will be even higher if the water levels on the reef flat are modelled more accurately, as the short wave heights across the Kwajalein reef flat strongly depends on the water depth on the reef flat. Combining these results and the expected rising of sea levels, it is expected the wave runup will increase in the future. Rising offshore water levels will result in less wave-induced setup on the reef flat, but will cause an increase in the amplitude of infragravity and incident swash magnitudes.

6.2 Recommendations

In this study insight is obtained on the wave runup at atoll reefs, which can be useful for further research. In this section the recommendations are presented for further research on wave runup at atoll reefs in general. This thesis is part of a broader study that investigates the influence of sea-level rise on wave driven inundation and the resulting impacts to infrastructure and freshwater resources on atoll islands in the Pacific and Indian Oceans. In addition to the general recommendations, recommendations are made regarding the broader study.

Applicability of hourly burst-averaged hydraulic conditions

From the model results it was concluded the hydrostatic XBeach model can accurately reproduce the hydrodynamics across the Kwajalein Atoll reef, but underestimates the peak wave runup event in November. However, there was only one peak runup event observed during the deployment period, so it is not known if the applicability of the burst-averaged water levels is insufficient for all peak wave runup events. Therefore, more observations of extreme wave runup events at atoll reefs are needed to investigate the exact processes causing such extreme runup events. Additionally, it is recommended to investigate whether the wave runup is only underestimated for the extreme event, or also for the more moderate wave runup observations. The other, less extreme, runup observations can be used for additional simulations. A more statistically based conclusion can be drawn on the performance of both models on wave runup at Kwajalein Atoll. Additionally, with these simulations the applicability of hourly burst-averaged hydraulic conditions for less extreme events can be tested.

XBeach hydrostatic versus non-hydrostatic

The main advantage of the XBeach hydrostatic model is that it is computationally less expensive with respect to the non-hydrostatic model. The XBeach hydrostatic model showed good results for the hydrodynamics across the reef, but the non-hydrostatic model performed better on the wave runup. Extrapolating these results to storm conditions, it is expected the incident swash component contributes significantly to the total wave runup, as the water depth on the reef flat increases and a shift into a more energetic band of forcing will occur. This effect was substantiated by the conceptual model simulations. Furthermore, the impact of incident swash is expected to become stronger considering the effects of rising sea levels. Therefore, it is recommended to use the XBeach non-hydrostatic model for simulating wave runup on atoll reefs. However, first, the underestimation of the water levels on the reef flat by XBeach non-hydrostatic model must be further investigated. If this issue can be solved, the model is capable to model the wave runup (and subsequently inundation events) more accurately.

Two-dimensional effects

This study focussed on the one-dimensional wave runup process on atoll reefs. However, wave runup is sensitive to the choice of dimensional space due to alongshore variations in bathymetry and bottom topography. Therefore, it is recommended to investigate the wave runup on an atoll reef in a two-dimensional space to identify the locations where potentially the highest wave runup, and subsequently inundation, will occur. Due to the physical size of atoll systems, it is not easy to investigate the wave runup on two-dimensional atoll system or island by field measurements. A numerical model such as XBeach can provide insight in the two-dimensional wave runup processes on an atoll reef.

Wave runup on atoll reefs in general

With the conceptual model a first indication of parameters affecting the wave runup were identified. However, these were identified by conducting numerical simulations and the number of simulations was limited by a using Kwajalein Atoll as a reference case. For example, the wave runup at a reef with relatively rougher bottom topography can respond differently to a variation in the offshore tidal elevation. To get a complete understanding of the processes and parameters affecting the wave runup on atoll reefs, measurements of wave runup are needed for a variety of atoll reefs. Idealistically, the same level of knowledge as is present for sandy coasts can be achieved for wave runup on (atoll) reef environments and a set of empirical relations for wave runup on (atoll) reefs is derived.

References

Battjes, J. A. (1974). Surf Similarity. In *Proceedings of the 14th Conference of Coastal Engineering.* (pp. 466–480).

Becker, J. M., Merrifield, M. A., & Ford, M. (2014). Water level effects on breaking wave setup for Pacific Island fringing reefs. *Journal of Geophysical Research Oceans*, *119*. doi:10.1002/2013JC009373

Bodde, W. (2013). *Sediment transport in a fringing reef environment. Analysis using laboratory experiments and numerical modelling*.

Darwin, C. (1842). *The structure and distribution of coral reefs. Being the first part of the geology of the voyage of the Beagle, under the command of Capt. Fitzroy, R.N. during the years 1832 to 1836.* London: Smith Elder and Co.

Ferrario, F., Beck, M. W., Storlazzi, C. D., Micheli, F., Shepard, C. C., & Airoldi, L. (2014). The effectiveness of coral reefs for coastal hazard risk reduction and adaptation. *Nature Communications*, *5*, 3794. doi:10.1038/ncomms4794

Gerritsen, F. (1980). Wave attenuation and wave set-up on a coastal reef. In *Proceedings of the 17th International Conference on Coastal Engineering* (pp. 444–461).

Gourlay, M. R. (1996). Wave set-up on coral reefs. 1. Set-up and wave-generated flow on an idealised two dimensional horizontal reef. *Coastal Engineering*, *27*, 161–193. doi:10.1016/0378-3839(96)00008-7

Hagan, A. B., & Spencer, T. (2008). Reef resilience and change 1998-2007 , Alphonse Atoll , Seychelles, (12), 7–11.

Hamylton, S. (2011). The use of remote sensing and linear wave theory to model local wave energy around Alphonse Atoll, Seychelles. *Estuarine, Coastal and Shelf Science*, *95*(4), 349–358. doi:10.1016/j.ecss.2011.08.035

Hoeke, R. K., McInnes, K. L., Kruger, J. C., McNaught, R. J., Hunter, J. R., & Smithers, S. G. (2013). Widespread inundation of Pacific islands triggered by distant-source wind-waves. *Global and Planetary Change*, *108*, 128–138. doi:10.1016/j.gloplacha.2013.06.006

Holland, K. T. (1995). Runup kinematics on a natural beach, *100*(section 4), 4985–4993.

Holman, R. A. (1986). Extreme value statistics for wave run-up on a natural beach. *Coastal Engineering*, *9*(6), 527–544. doi:10.1016/0378-3839(86)90002-5

Holthuijsen, L. H. (2007). *Waves in oceanic and coastal waters*. Cambridge University Press.

Huang, Z. C., Reineman, B., Lenain, L., Melville, W. K., & Middleton, J. H. (2012). Airborne Lidar Measurements of Wave Energy Dissipation in A Coral Reef Lagoon System. *Journal of Geophysical Research*, *117*.

Hunt, I. A. (1959). Design of seawalls and breakwaters. *Journal of Waterways and Harbours Division*, *85*, 123–152.

Jago, O. K., Kench, P. S., & Brander, R. W. (2007). Field observations of wave-driven water- level gradients across a coral reef flat. *Journal of Geophysical Research Oceans*, *112*(C6).

Jensen, O. J. (1991). Waves On Coral Reefs. *Coastal Zone*, *91*(7th Symp. On Coastal and Ocean Management, Long Beach, Calif. 8-12 July 1991).

Lee, T. T., & Black, K. P. (1978). The energy spectra of surf waves on a coral reef. In *Proc.16th Int. Conf. Coastal Eng.*

Longuet-Higgins, M. S., & Stewart, R. W. (1962). Radiation stress and mass transport in gravity waves, with application to “surf beats”. *Journal of Fluid Mechanics*, *13*, 481–504.

Lowe, R. J., Falter, J. L., Bandet, M. D., Pawlak, G., Atkinson, M. J., Monismith, S. G., & Koseff, J. R. (2005). Spectral wave dissipation over a barrier reef. *Journal of Geophysical Research*, *110*(C4). doi:10.1029/2004JC002711

McCall, R. T., van Thiel de Vries, J. S. ., Plant, N. G., van Dongeren, A. R., Roelvink, J. A., Thompson, D. M., & Reniers, A. J. H. M. (2010). Two-dimensional time dependent hurricane overwash and erosion modeling at Santa Rosa Island. *Coastal Engineering*, *57*, 668–683.

Munk, W. H., & Sargent, M. C. (1948). Adjustments of Bikini Atoll to ocean waves. *Transactions of the American Geophysical Union*, *29*, 855–860.

Nwogu, O., & Demirbilek, Z. (2010). Infragravity Wave Motions and Runup over Shallow Fringing Reefs. *Journal of Waterway, Port, Coastal and Ocean Engineering*, *136*, 295–305.

Péquignet, a. C. N., Becker, J. M., Merrifield, M. a., & Aucan, J. (2009). Forcing of resonant modes on a fringing reef during tropical storm Man-Yi. *Geophysical Research Letters*, *36*(3), L03607. doi:10.1029/2008GL036259

Péquignet, a. C. N., Becker, J. M., Merrifield, M. A., & Boc, S. J. (2011). The dissipation of wind wave energy across a fringing reef at Ipan, Guam. *Coral Reefs*, *30*, 71–82.

Pomeroy, A., Lowe, R. J., Symonds, G., van Dongeren, A. R., & Moore, C. (2012). The dynamics of infragravity wave transformation over a fringing reef. *Journal of Geophysical Research*, *117*, C11022. doi:10.1029/2012JC008310

Presto, M. K., Ogston, A. S., Storlazzi, C. D., & Field, M. E. (2006). Temporal and spatial variability in the flow and dispersal of suspended- sediment on a fringing reef flat, Molokai, Hawaii. *Estuar Coast Shelf Sci*, *67*, 67–81.

Raubenheimer, B., Guza, R. T., Elgar, S., & Kobayashi, N. (1995). Swash on a gently sloping beach, *100*, 8751–8760.

Roelvink, J. A. (1993). Dissipation in random wave groups incident on a beach. *Coastal Engineering*, *19*, 127– 150.

Roelvink, J. A., Reniers, A., van Dongeren, A. R., van Thiel de Vries, J., McCall, R., & Lescinski, J. (2009). Modelling storm impacts on beaches, dunes and barrier islands. *Coastal Engineering*, *56*(11-12), 1133–1152. doi:10.1016/j.coastaleng.2009.08.006

Roelvink, J. A., & Stive, M. J. F. (1989). Bar-generating cross-shore flow mechanisms on a beach. *Journal of Geophysical Research*, *94*(C4), 4785–4800.

Ruessink, B. G., Miles, J. R., Feddersen, F., Guza, R. T., & Elgar, S. (2001). Modeling the alongshore current on barred beaches. *Journal of Geophysical Research*, *106*, 22451–22463.

Seelig. (1983). Laboratory study of reef-lagoon system hydraulics. *Journal of Waterway, Port, Coastal and Ocean Engineering*, *109*(4), 380–391.

Smit, P. B. (2008). *Non-hydrostatic modelling of large scale tsunamis*. Delft University of Technology.

Stelling, G. S., & Zijlema, M. (2003). An accurate and efficient finite-difference algorithm for non-hydrostatic free-surface flow with application to wave propagation. *Int. J. Numer. Meth. Fluids*, *43*, 1–23.

Stockdon, H. F., Holman, R. A., Howd, P. A., & Sallenger, A. H. (2006). Empirical parameterization of setup, swash, and runup. *Coastal Engineering*, *53*(7), 573–588. doi:10.1016/j.coastaleng.2005.12.005

Stockdon, H. F., Thompson, D. M., Plant, N. G., & Long, J. W. (2014). Evaluation of wave runup predictions from numerical and parametric models. *Coastal Engineering*, *92*, 1–11. doi:10.1016/j.coastaleng.2014.06.004

Storlazzi, C. D., Elias, E., Field, M. E., & Presto, M. K. (2011). Numerical modeling of the impact of sea-level rise on fringing coral reef hydrodynamics and sediment transport. *Coral Reefs*, *30*(S1), 83–96. doi:10.1007/s00338-011-0723-9

Storlazzi, C. D., Ogston, A. S., Bothner, M. H., Field, M. E., & Presto, M. K. (2004). Wave- and tidally-driven flow and sediment flux across a fringing coral reef: Southern Molokai, Hawaii. *Continental Shelf Research*, *24*(12), 1397–1419. doi:10.1016/j.csr.2004.02.010

Symonds, G., Huntley, D. A., & Bowen, A. J. (1982). Long Wave Generation by a Time-Varying Breakpoint, *87*(1), 492–498.

Tait, R. J. (1972). Wave set-up on coral reefs. *Journal of Geophysical Research*, *77*(12), 2207–2211.

Tartinville, B., & Rancher, J. (2000). Wave-induced flowover Mururoa Atoll Reef. *Journal of Coastal Research*, *16*(3), 776–781.

TAW. (2002). *Technical Report - Wave runup and wave overtopping at dikes*. Delft.

Van Dongeren, A. R., Battjes, J. A., Janssen, T., van Noorloos, J., Steenhauer, K., Steenbergen, G., & Reniers, A. J. H. M. (2007). Shoaling and shoreline dissipation of low-frequency waves. *Journal of Geophysical Research*, *112*(C02011). doi:10.1029/2006JC003701

Van Dongeren, A. R., Lowe, R. J., Pomeroy, A., Trang, D. M., Roelvink, J. A., Symonds, G., & Ranasinghe, R. (2013). Numerical modeling of low-frequency wave dynamics over a fringing coral reef. *Coastal Engineering*, *73*, 178–190. doi:10.1016/j.coastaleng.2012.11.004

Van Dongeren, A. R., Reniers, A. J. H. M., & Battjes, J. A. (2003). Numerical modeling of infragravity wave response during DELILAH. *Journal of Geophysical Research*, *108*(C9), 3288. doi:10.1029/2002JC001332

Vetter, O., Becker, J. M., & Merrifield, M. A. (2010). Wave setup over a Pacific Island fringing reef. *Journal of Geophysical Research*, *115*, C12066. doi:10.1029/2010JC006455

Young, I. R. (1989). Wave transformation over coral reefs. *Journal of Geophysical Research*, *94*(C7), 9779–9789.

Zijlema, M., & Stelling, G. S. (2008). Efficient computation of surf zone waves using the nonlinear shallow water equations with non-hydrostatic pressure. *Coastal Engineering*, *55*(10), 780–790. doi:10.1016/j.coastaleng.2008.02.020

Zijlema, M., Stelling, G. S., & Smit, P. B. (2011). SWASH: An operational public domain code for simulating wave fields and rapidly varied flows in coastal waters. *Coastal Engineering*, *58*(10), 992–1012.

A Additional XBeach hydrostatic results

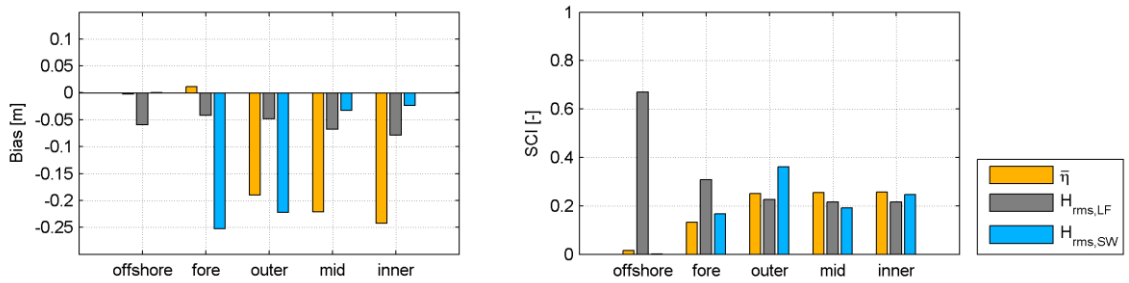

Figure B.1 Bias and SCI for simulation C2

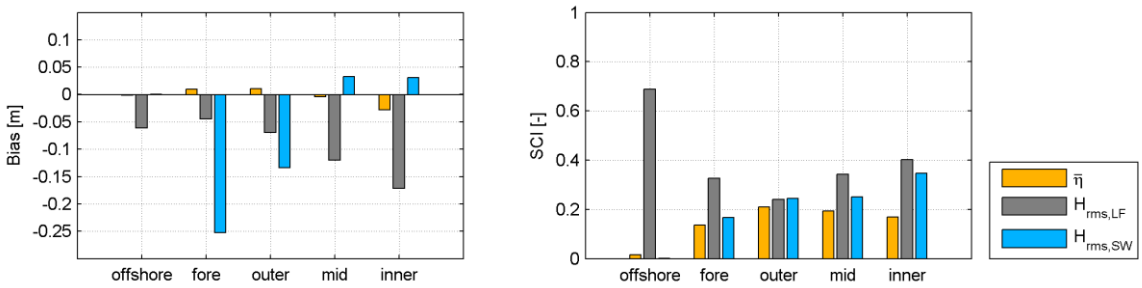

Figure B.2 Bias and SCI for simulation C3

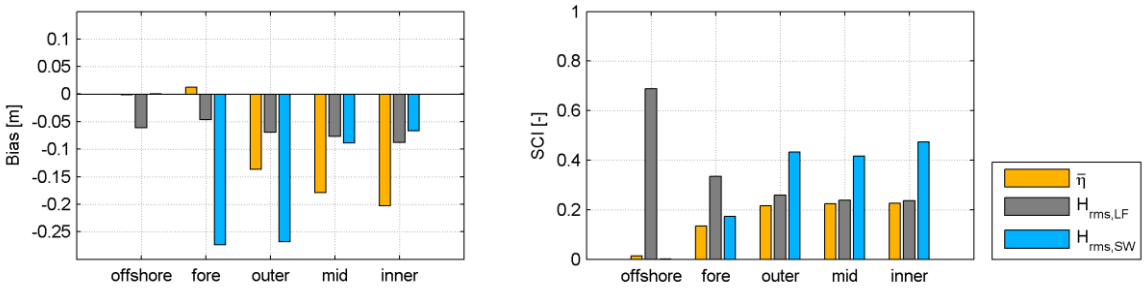

Figure B.3 Bias and SCI for simulation C4